Study Of Photovoltaic Solar Cell Technologies and Numerical Simulation Analysis of State of Art Perovskite Solar Cell

Dissertation submitted to
Visvesvaraya National Institute of Technology, Nagpur
in partial fulfilment of the requirements for the award of
the degree

Master of Science

in

Physics

by

Aman Yadav (MS23PHY013)

under the guidance of

Dr. Sushama M Giripunje

Department of Physics

Visvesvaraya National Institute of Technology

Nagpur 440 010 (India)

May 2025

Study Of Photovoltaic Solar Cell Technologies and Numerical Simulation Analysis of State of Art Perovskite Solar Cell

Dissertation submitted to
Visvesvaraya National Institute of Technology, Nagpur
in partial fulfilment of the requirements for the award of
the degree

Master of Science

in

Physics

by

Aman Yadav (MS23PHY013)

under the guidance of

Dr. Sushama M Giripunje

Department of Physics

Visvesvaraya National Institute of Technology

Nagpur 440 010 (India)

May 2025

© Visvesvaraya National Institute of Technology (VNIT) 2025

Department of Physics

Visvesvaraya National Institute of Technology, Nagpur

Declaration

I, **Aman Yadav**, hereby declare that this dissertation titled **"Study of photovoltaic solar cell technologies and numerical simulation analysis of state of art perovskite solar cell"** is carried out by me in the Department of Physics of Visvesvaraya National Institute of Technology, Nagpur. The work is original and has not been submitted earlier whole or in part for the award of any degree/diploma at this or any other Institution / University.

Aman Yadav

Date:

Certificate

This to certify that the dissertation titled "**Study of photovoltaic solar cell technologies and numerical simulation analysis of state of art perovskite solar cell**" is submitted by **Aman Yadav** in partial fulfilment of the requirements for the award of the degree of **Master of Science in Physics**, VNIT Nagpur. The work is comprehensive, complete and fit for final evaluation.

Dr. Sushama M Giripunje

Associate Professor

Department of Physics

VNIT, Nagpur

Head, Department of Physics

VNIT, Nagpur

Date

Department of Physics

Visvesvaraya National Institute of Technology, Nagpur

Non-Plagiarism Certificate

Certified that M. Sc. Dissertation titled **"Study of photovoltaic solar cell technologies and numerical simulation analysis of state of art perovskite solar cell"** submitted by **Aman Yadav**, Enrolment no. **MS23PHY013,** ID No.**30322** has been checked for plagiarism using TURNITIN software and overlap is found within prescribed limits (< 30%). A summary of the report given below:

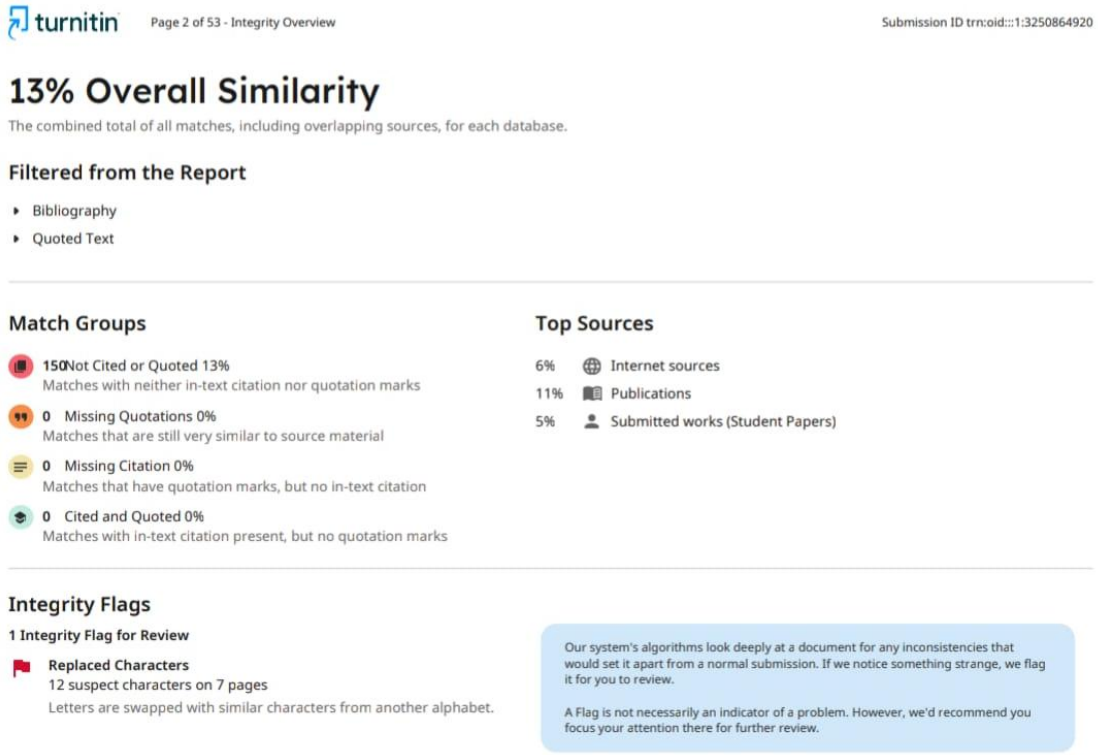
turnitin Page 2 of 53 - Integrity Overview Submission ID trn:oid:::1:3250864920

13% Overall Similarity

The combined total of all matches, including overlapping sources, for each database.

Filtered from the Report

- Bibliography
- Quoted Text

Match Groups

150 Not Cited or Quoted 13%
Matches with neither in-text citation nor quotation marks

0 Missing Quotations 0%
Matches that are still very similar to source material

0 Missing Citation 0%
Matches that have quotation marks, but no in-text citation

0 Cited and Quoted 0%
Matches with in-text citation present, but no quotation marks

Top Sources

6% Internet sources
11% Publications
5% Submitted works (Student Papers)

Integrity Flags

1 Integrity Flag for Review

Replaced Characters
12 suspect characters on 7 pages
Letters are swapped with similar characters from another alphabet.

Our system's algorithms look deeply at a document for any inconsistencies that would set it apart from a normal submission. If we notice something strange, we flag it for you to review.

A Flag is not necessarily an indicator of a problem. However, we'd recommend you focus your attention there for further review.

Aman Yadav

(MS23PHY013)

ID No: 30322

Dr. Sushama M Giripunje

Associate Professor

Department of Physics

VNIT, Nagpur

Acknowledgements

I would like thank from bottom of my heart **Dr. Sushama M Giripunje**, Associate professor, Department of Physics, Visvesvaraya National Institute of Technology Nagpur, for guiding me and providing me the opportunity to do my project under her wisdomful guidance. I have learned so much about the solar energy from this learning experience. She has always guided me and listened to my problems like a parent.

I would really like give my special thanks to **Mr. Alok Kumar Verma**, Research Scholar, Department of Physics VNIT, for supporting and guiding me on from very basic things to advanced level ideas throughout this project journey. His experience and wisdom have helped me a lot.

I would also like to heartfully thank **Dr. B R Sankpal,** Head of the Department of Physics, VNIT for providing and permitting access to all the facilities that were necessary for this project work.

Further, I want to express my gratefulness for my parents, my family members and my friends for being supportive in my project journey.

Aman Yadav

Abstract

This study investigates the application of Copper Barium Tin Sulfide (CBTS) as hole transport layer (HTL) in $FASnI_3$-based PSCs (perovskite solar cells). Traditional organic HTLs, such as PEDOT: PSS and Spiro-OMeTAD, exhibit issues including poor thermal stability, susceptibility to degradation, chemical incompatibility, and low intrinsic hole mobility. This study investigates the capability of Cu_2BaSnS_4 (CBTS) as a viable material to mitigate existing limitations, assessing its suitability for enhanced photovoltaic performance and stability. Using the SCAPS-1D simulator, a cell structure of $Au/CBTS/FASnI_3/TiO_2/FTO/Al$ attained superior efficiency of 26.67%, J_{SC} (short-circuit current density) of 29.21 mA/cm^2, with an V_{OC} (open-circuit voltage) of 1.097 V, and an FF (fill factor) of 83.20%. In this work author analysed the diagram of energy band levels and studied the influence on PV parameters because of, acceptor density, thickness, contact work functions, radiative recombination, and defect density, temperature, electron affinity, Mott-Schottky plot and resistances. This work highlights the advantages of PSCs that are free from Pb and opens new avenues for their application in advanced photovoltaic technologies such as tandem solar cells.

List of Figures

Figure No.	Title	Page No.
1	Renewable Energy sources	2
2	Generations of solar cells	5
3	**(a)** Silicon solar cell module, **(b)** Layered structure of Silicon solar cells, **(c)** Polycrystalline and Monocrystalline solar cells, **(d)** Bifacial solar cell.	6
4	**(a)** PV cell**, (b)** PV Module**, (c)** PV panel and **(d)** Array	7
5	**(a)** Layered structure of Thin Film Solar Cells, (b) CIGS Solar Cell, **(c)** GaAs Solar Cell, **(d)** Amorphous Silicon Solar Cell.	8
6	**(a)** Perovskite Solar Cell, **(b)** Dye Sensitized Solar Cell, **(c)** Organic Solar Cell, **(d)** Quantum Dot Solar Cell	10
7	**(a)** Cubic cell structure of Perovskite material and **(b)** crystallographic structure of Perovskite material	13
8	Device Architecture of Perovskite Solar Cells	15
9	CH3NH3PbI3 perovskite Solar Cell	20
10	Front Panel of SCAPS 1D software	25
11	**(a)** Schematic diagram of the suggested perovskite PV cell with CBTS as HTL and **(b)** Unit cell structure of $FASnI_3$	26
12	nalysis of **(a)** J-V characteristics **(b)** energy band diagram **(c)** bsorber layer (FASnI3) thickness on quantum efficiency and **(d)** ffect of absorber layer thickness on J-V characteristics.	32
13	Contour mapping analysis of back contact metal work function and front contact work function on **(a)** efficiency **(b)** fill factor, **(c)** current density and **(d)** voltage.	34
14	**(a)** Effect of temperature on PV parameters, **(b)** & **(c)** effect of acceptor density of absorber layer on PV parameters.	36

15	Effect of shunt and series resistance on **(a)** efficiency, **(b)** fill factor, **(c)** current density and **(d)** voltage	38
16	Equivalent diode model circuit of the solar cells	39
17	Effect of **(a)** interface defect density (HTL/Absorber layer) and **(b)** total defect density of absorber layer on PV parameters	40
18	**(a)** Effect of electron affinity on PV parameters, **(b)** C-V characteristics **(c)** Mott-Schottky plot.	42
19	**(a)** Impact of radiative recombination coefficient on J_{SC} and η (%) and **(b)** Impact of radiative recombination coefficient on V_{OC} and FF.	43

List of Tables

Figure No.	Title	Page No.
1	Optimised SCAPS parameter.	29
2	Comparison between present work and work done by other researchers.	44

List of Abbreviation

Abbreviation	Full form
PV	Photovoltaic
DC	Direct Current
CdTe	Cadmium Telluride
CIGS	Copper Indium Gallium Di-Selenide
GaAs	Gallium Arsenide
DSSCs	Dye-Sensitized Solar Cells
OPVs	Organic Photovoltaics
a-SiC	Amorphous Silicon Carbide
c- Si	Crystalline Silicon
PSCs	Perovskite Solar Cells
PCEs	Power Conversion Efficiencies
Sn	Tin
$CaTiO_3$	Calcium Titanate
Spiro-OMeTAD	Spiro-methoxy-substituted triarylamine derivative
NREL	National Renewable Energy Laboratory
SnO_2	Tin Oxide
CH_3NH_3	methylammonium
FTO	Fluorine-doped Tin Oxide
HTL	Hole Transport Layer
ETL	Electron Transport Layer
PEDOT: PSS	Poly(3,4-ethylenedioxythiophene): Poly(styrenesulfonate)
Li-TFSI	Lithium bis(trifluoromethanesulfonyl)imide
tBP	tert-Butylpyridine
DSSCs	Dye Sensitized Solar Cells
TiO_2	Titanium Dioxide
$CH_3NH_3PbI_3$	methylammonium lead iodide

$CH_3NH_3PbBr_3$	methylammonium lead bromide
Al_2O_3	alumina scaffold
DLTs	dynamic leaching tests
TCLP	Toxicity Characteristic Leaching Procedure
SPLP	Synthetic Precipitation Leaching Procedure
TOC	total organic carbon
$CH_3NH_3SnI_3$	methylammonium tin iodide
$MASnI_3$	Methylammonium Tin Iodide
$FASnI_3$	Formamidinium Tin Iodide
ZnO,	Zinc Oxide
PCBM	[6,6]-Phenyl-C61-butyric acid methyl ester
CuI	Copper(I) Iodide
CuSCN	Copper(I) Thiocyanate
CBTS	Copper Barium Tin Sulfide
$CsPbI_3$	Cesium Lead Iodide
IGZO	Indium Gallium Zinc Oxide
DFT	Density Functional Theory
$CsSnCl_3$	Cesium Tin Chloride
BPVE	Bulk Photovoltaic Effect

List of Symbols and Meaning

Symbol	Meaning
η	Photoconversion efficiency
I_{sc}	Short circuit current
V_{oc}	Open circuit voltage
FF	Fill factor
I_{MP}	Current at Maximum Power
V_{MP}	Voltage at Maximum Power
P_{max} / P_{out}	Maximum output power

INDEX

Section	Title	Page No.
	Abstract	i
	List of Figures	ii
	List of Tables	iii
	List of Abbreviations	iv
	List of Symbols	vii
	Contents	viii
1	INTRODUCTION	1
1.1	Sources for Renewable Energy	2
1.2	Solar Cells	3
1.3	Photovoltaic Effect and History of Solar Cells	4
1.4	Generations of Solar Cells	4
1.4.1	First Generation of Solar Cells	5
1.4.2	Second Generation of Solar Cells	8
1.4.3	Third Generation of Solar Cells	9
1.4.4	Fourth Generation of Solar Cells	10
1.5	Perovskite Solar Cells	11
1.5.1	Perovskite and History of Perovskite Solar Cells	11
1.5.2	Perovskite Structure	13
1.5.3	Working Principle of Perovskite Solar Cells	14
2	LITERATURE SURVEY	17

Section	Title	Page No.
2.1	First Ever Perovskite Solar Cell and Early Developments	18
2.2	Lead-free Perovskite Solar Cells	20
2.3	Study of Different HTLs and ETLs used in Perovskite Solar Cells	22
3	DEVICE STRUCTURE AND SIMULATION METHODOLOGY	24
3.1	Introduction to SCAPS 1D Simulation	25
3.2	Device Structure	26
3.3	Simulation Methodology and Optimised Input Parameters	27
4	RESULT AND DISCUSSION	30
4.1	Analysis of J-V Characteristics	31
4.2	Quantum Efficiency and Band Diagram Analysis	32
4.3	Impact of Work Function	34
4.4	Effect of Temperature and Acceptor Density	35
4.5	Impact of Series and Shunt Resistance	37
4.6	Impact of Interface Defect Density and Total Defect Density	39
4.7	Impact of Electron Affinity and C-V Analysis	41
4.8	Impact of Radiative Recombination Coefficient	42
5	SUMMARY AND CONCLUSION	45
5.1	Summary	46
5.2	Conclusion and Future Scope	47
-	REFERENCES	48

CHAPTER 1: INTRODUCTION

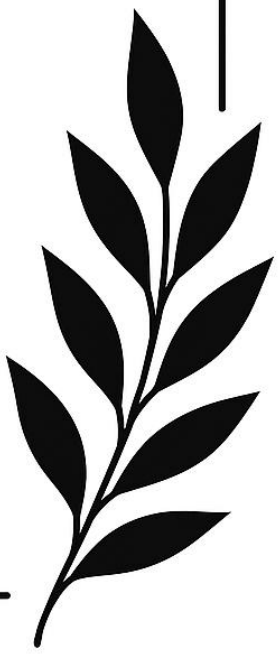

CHAPTER 1: INTRODUCTION

1.1 Sources for Renewable Energy

Renewable sources of energy are the natural sources that are continuously recurring and are sustainable over a long time. The energy extracted from these sources is renewable energy. The primary types of renewable energy are :solar energy, which harnesses sunlight using solar cells and solar thermal energy is also utilized ; wind energy, which generated through windmill that converts wind movement into electricity; hydropower, that utilizes the flow of water in rivers or dams to produce energy; biomass energy, that is extracted out of organic materials like plant remains, crop remains, and animal manure that can be combusted or processed to yield electricity, heat, or biofuels; geothermal energy, which uses Earth's inner heat for power or heating directly; and ocean energy, utilizing wave, and ocean thermal energy that harnesses tidal movements and temperature differences .

Fig 1. Renewable Energy Sources [1]

These sources are cleaner substitutes of fossil fuels, notably reducing the greenhouse gas emissions, and are essential for achieving sustainability over period of time [2]. Although

other renewable sources namely hydro, wind, and geothermal have their advantages, solar energy stands out as a leading renewable resource due to its decreasing costs [3], environmental benefits [4], energy security [5] and scalability [6]. Solar energy is the radiant energy radiated from the sun, which can be utilized and transformed into operational forms of power, namely as heat and electricity, through innovative technologies like photovoltaic (PV) panels and solar thermal systems. This renewable energy source is not only sustainable and abundant but also very environmentally friendly, providing a reliable alternative to traditional fossil fuels. Over the past few years, the adoption of solar energy has been accelerating globally because of significant technological advancements, decreasing costs, and an increasing awareness of the urgent need to address climate change. Governments, businesses, and individuals are increasingly recognizing the benefits of solar energy, which includes reduced emissions of the greenhouse gases, energy independence, and creation of job in the green economy sector. As we move forward, solar energy is set to play a pivotal role in the transition to a more sustainable energy future [7].

1.2 Solar Cells

A solar cell, or photovoltaic (PV) cell, is a semiconductor device which is intended to capture sunlight and transform it directly into electricity by the photovoltaic effect. Main of its operation is the p-n junction, created by 2 layers of semiconducting material. One layer, known as the p-type layer, is doped to possess an overabundance of positive charge carriers, while the other n-type layer has an overabundance of negative charge carriers. When sunlight, comprised of photons, strikes the solar cell, it energizes the e^- within the semiconductor, resulting in the formation of pairs of negatively charged e^- and positively charged h^+. The built-in field is very crucial; it acts as a selective barrier that efficiently separates these charge carriers. This separation propels the e^- toward the n-type layer and the h^+ toward the p-type layer, creating a notable voltage difference across the cell. To effectively harness this electrical energy, metal contacts placed on the top and bottom surfaces collect the freed electrons, allowing them to flow through an external circuit and generate a steady stream of direct current (DC) electricity [8]. To maximize power output, individual solar cells are interconnected into the larger units called modules. These modules can be further organized into extensive arrays, significantly boosting energy production and establishing solar technology as a key player in the modern renewable

energy landscape [9]. Solar cells offer a clean, sustainable alternative to fossil fuels, substantially adding to the reduction of greenhouse gases and facilitating the shift towards an eco-friendlier future. Ongoing research and development is focused on enhancing solar cell efficiency, lowering production costs, and exploring innovative materials. This ensures that solar technology remains at the forefront of renewable energy solutions and continues to grow in its application across various regions and sectors worldwide.

1.3 Photovoltaic Effect and History of Solar Cells

The effect known as photovoltaic effect, a groundbreaking phenomenon was first discovered in the year of 1839 by the Edmond Becquerel, physicist from French. It describes the generation of electric current that occurs when certain materials are exposed to light, effectively turning photons into usable energy. Becquerel made this remarkable observation while experimenting with an electrolytic cell, marking an important step in the exploration of solar energy [10]. However, it wasn't until 1873, when the British scientist Willoughby Smith noticed photoconductivity in selenium, that the potential for solar technology gained significant traction [11]. Building on this foundation, Charles Fritts created the first true solar cell in 1883 with PCE of about 1 % , utilizing selenium coated with a thin layer of gold, which represented a significant advancement in the field [12]. A further step forward was in 1905 when Albert Einstein issued his explanation for the photoelectric effect, a theoretical framework that ultimately secured him the Nobel Prize in Physics in 1921 [13] and laid the groundwork for the understanding of how light interacts with matter to produce electricity. The development of practical silicon-based solar cells in 1954 at Bell Labs by researchers Daryl Chapin, Calvin Fuller, and Gerald Pearson, who achieved an efficiency of 6% [14], this marked the true birth of modern photovoltaic technology, paving the way for the advancement of solar energy solutions that we continue to rely on today. Since then, a lot of research has been done on the solar cells and different generations of solar cells are witnessed over the time.

1.4 Generations of Solar Cells

Classification of Solar cells are based on their structural and functional properties which affect light absorption and charge separation processes. They are also grouped into generations reflecting their historical development and construction materials. So far, four generations of solar cells have been developed [15]. The first generation includes wafer-based crystalline silicon solar cells, comprising monocrystalline, polycrystalline cells.

The second generation features thin-film technologies like CIGS (copper indium gallium selenide), CdTe (cadmium telluride), a-Si (amorphous silicon), and GaAs (gallium arsenide), known for their flexibility and lower production costs [16]. The third generation introduces some of the advanced innovations like perovskite solar cells, DSSCs (dye-sensitized solar cells), quantum dot solar cells and OPVs (organic photovoltaics) which, despite their promise and high efficiency, have not yet reached large-scale commercial production [17]. Fourth-generation solar cells are the newest hybrid photovoltaic devices that integrate organic materials, such as polymers, with inorganic nanomaterials like graphene, carbon nanotubes, and metal oxides. These cells leverage nanostructures to improve light absorption and charge transport [17]. Currently, they are primarily in the research phase but hold great promise for future commercial applications.

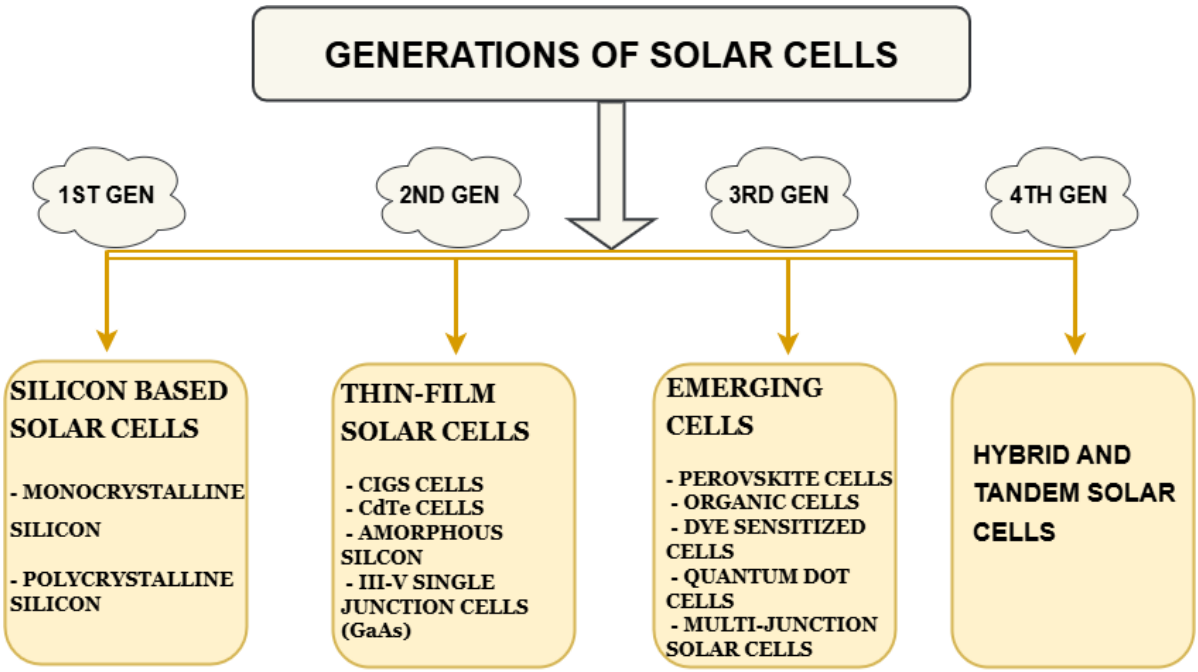

Fig 2. Generations of Solar Cell

1.4.1 First Generation of Solar Cells

Monocrystalline (Mono-Si) and polycrystalline (Poly-Si) silicon are the two main variants of first-generation solar cells, which are built on c-Si (crystalline silicon) and are the earliest and mostly used PV technology. With operating lives exceeding 25 years [18], these cells provide long-term stability and high-power conversion efficiencies based on well-established p-n junction principles. Their success is attributed to silicon's non-toxicity, abundance, and well-established production techniques, such as casting for Poly-

Si and the Czochralski method for Mono-Si. However, their intrinsic stiffness, energy-intensive manufacture, and stringent material purity requirements limit their use in flexible or lightweight photovoltaics. Because of its scalability and dependability, first-generation cells continue to dominate the worldwide solar market, accounting for about 90% of sales, despite these disadvantages [19]. While emerging technologies are also promising higher efficiencies and novel form factors, first-generation cells proceed to do a pivotal job in production of large-scale solar cells.

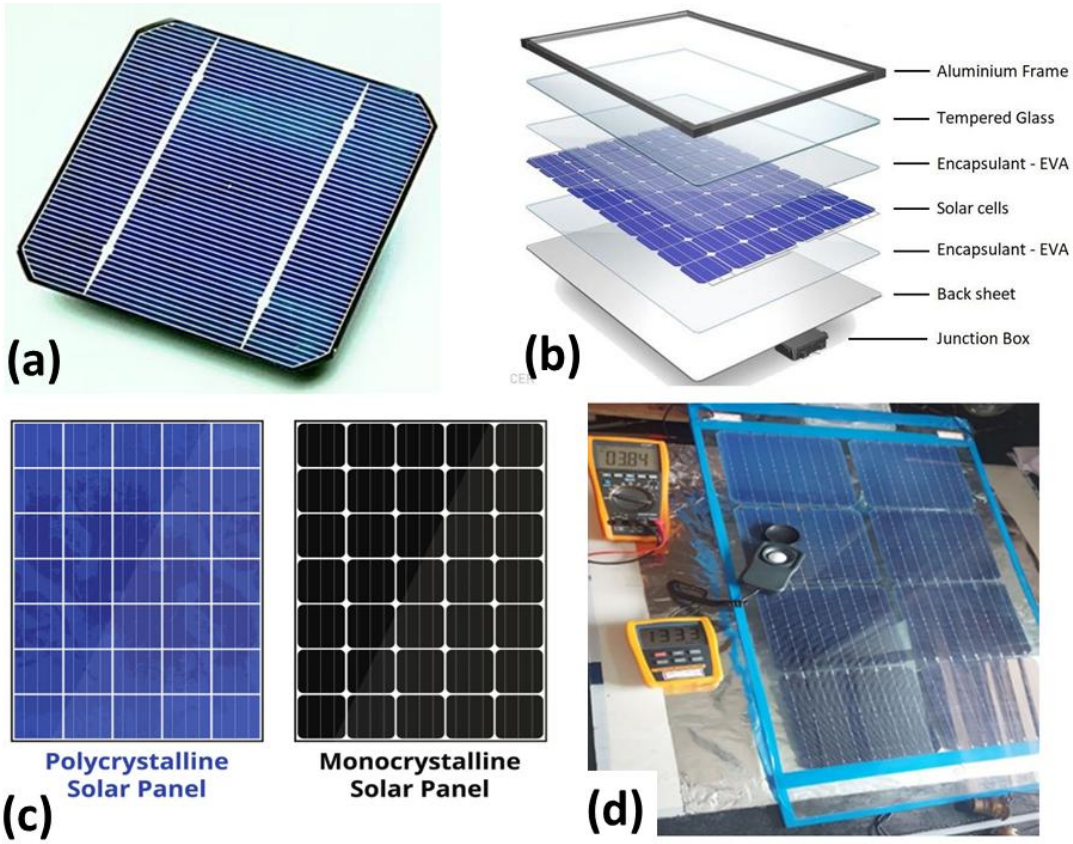

Fig 3. (a) Silicon solar cell [20]**, (b) Layered structure of Silicon solar cells** [21]**, (c) Polycrystalline and Monocrystalline solar modules** [22]**, (d) Bifacial solar module.**

The metallic connections known as bus bars and fingers in a solar cell are made to effectively gather and transfer the electrical current produced by sunlight. As seen in figure 3. (a), fingers are the thin, tightly spaced lines that are visible on the cell's surface. The electrons produced by the photovoltaic effect in the silicon layer are collected by these thin metallic strips. Their extreme narrowness reduces shade on the active surface, increasing the amount of sunlight that may be absorbed. The thicker metallic lines that often cross the cell are called bus bars, and the fingers direct the accumulated current to them. The

accumulated current is transported from the fingers to the external circuit by bus bars, which act as the primary conductors.

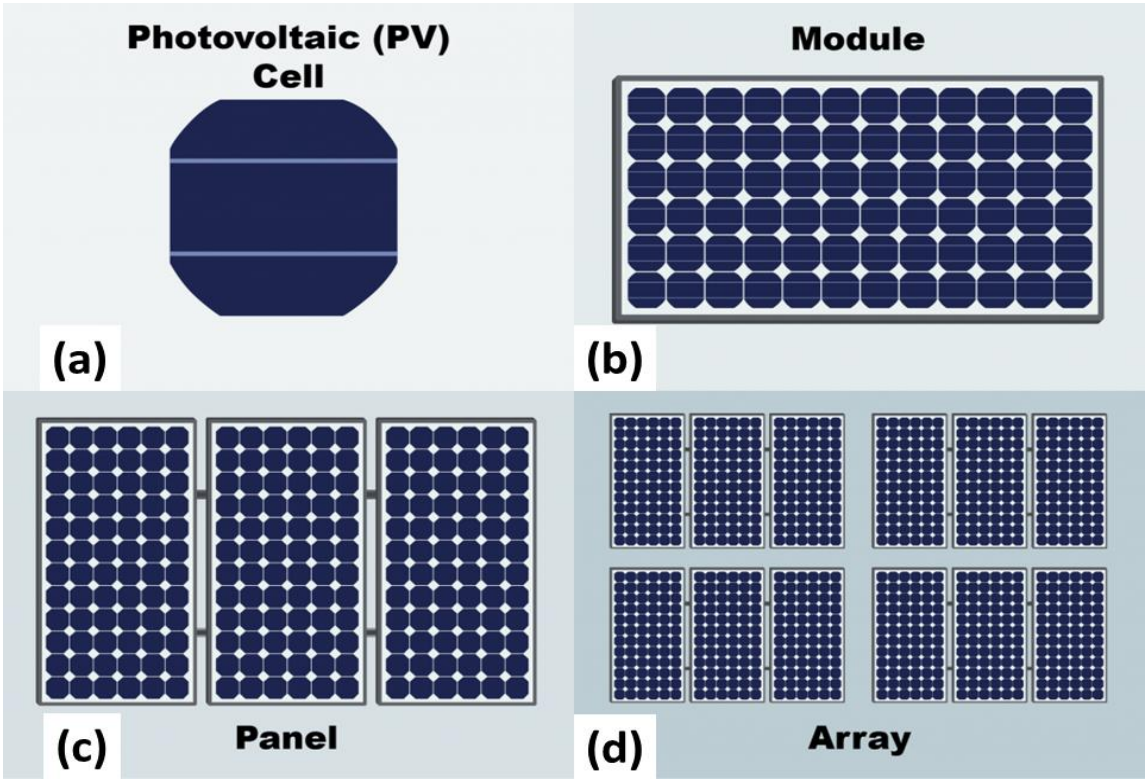

Fig 4. (a) PV cell, (b) PV Module, (c) PV panel and (d) Array

As we can see the, Fig.4 shows the hierarchical structure of a PV power generation system. It begins with the PV cell as shown in the figure 4. (a), the basic semiconductor device that converts the sunlight directly into direct current electricity through the well-known photovoltaic effect. Multiple photovoltaic cells are connected, usually it is in series connection and protected within modules made of materials like glass, EVA, and backsheet, forming a solar module as shown in figure 4. (b). The module, combined with other modules, creates a solar panel as shown in figure 4. (c) organised to produce specific voltage and current outputs. Several panels are then interconnected through series or parallel or both to form a solar array, which can be scaled to fulfil different power, voltage, and current requirements for grid-connected systems or for the off-grid systems. This design improves system scalability, energy optimization, and user-friendly maintenance.

1.4.2 Second Generation of Solar Cells

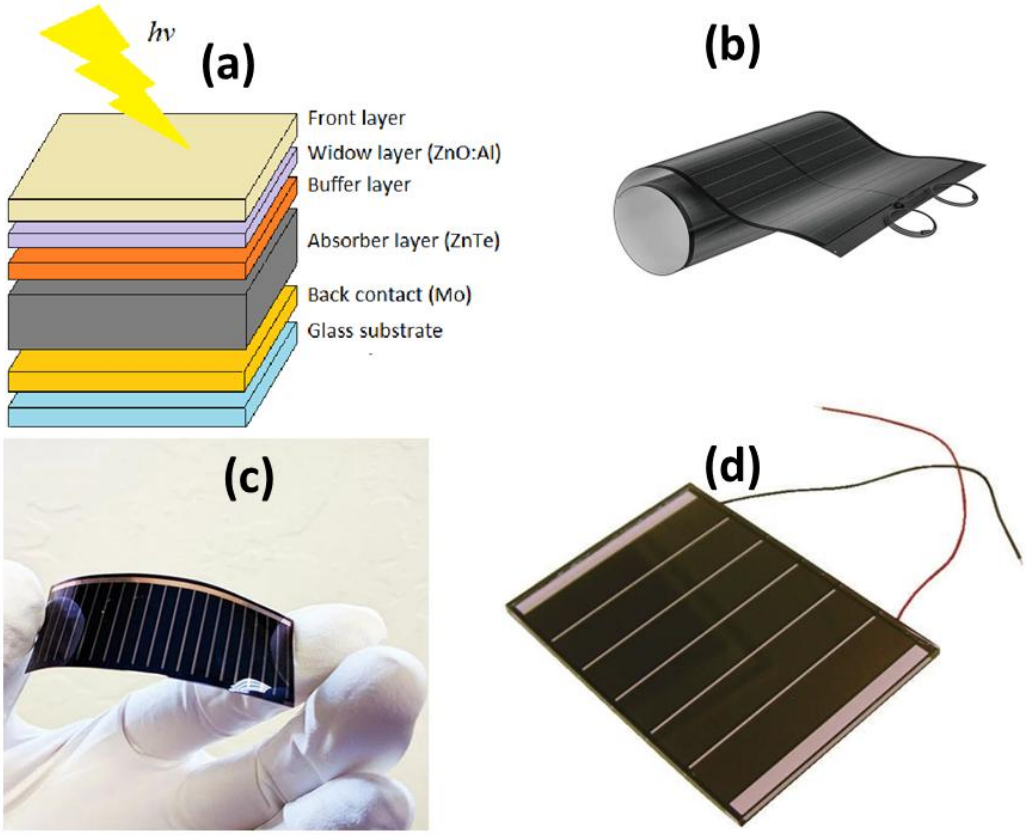

Fig 5. (a) Layered structure of Thin Film Solar Cells [23]**, (b) CIGS Solar Cell** [24]**, (c) GaAs Solar Cell** [25]**, (d) Amorphous Silicon Solar Cell** [26]**.**

By solving some of the shortcomings of conventional Si-based PV cells, such as their stiff construction and high material prices, 2nd-generation solar cells also called thin-film solar cells represent a substantial development in photovoltaic technology [27]. In order to create lighter, more adaptable, and more affordable solar modules, these cells use thin layers of photovoltaic materials, such as CIGS (copper indium gallium selenide), CdTe (cadmium telluride), and a-Si (amorphous silicon), placed on flexible or rigid substrates. A shorter energy payback period and better scalability are the results of the reduced material consumption and less energy-intensive manufacturing methods. Even though CdTe and CIGS cells typically have lesser efficiency than first-generation silicon cells, continuous research has resulted in continual increases, and today they can achieve lab efficiencies of over 22% [28]. They are also appropriate for a range of applications due to their better temperature coefficients and performance in low light [29]. To assure sustainable deployment, however, issues like the lack of some raw minerals (such indium and tellurium) and environmental issues with cadmium use call for more advancements in

material science and recycling methods. Second-generation solar cells continue to be a viable substitute in spite of these obstacles, providing a balance between cost, efficiency, and adaptability for the next renewable energy systems.

1.4.3 Third Generation of Solar Cells

Third-generation solar cells represent a very transformative step in photovoltaics, designed to exceed conventional efficiency limits while offering remarkable material versatility and device functionality. This diverse category includes perovskite-based PVCs, organic PVCs, dye-sensitized configurations, quantum dot systems, and advanced multi-junction designs, all of which uses novel light-matter interactions beyond traditional semiconductor physics. Perovskite solar cells, in particular, have revolutionized the field because of their exceptional optoelectronic properties like tunable bandgaps, long carrier diffusion lengths, and like high absorption coefficients [30]. However, the commercial viability of PSCs hinges on addressing intrinsic structural problems such as halide oxidation, ion migration, and phase segregation , prompting the development of advanced passivation strategies and stabilized formulations [31]. Concurrently, innovations in organic photovoltaics have produced non-fullerene acceptor systems with PCEs exceeding 19% [28], showcasing a exceptional electronic tunability through molecular engineering while maintaining the mechanical flexibility suitable for roll-to-roll processing. Quantum dot photovoltaics utilize size-dependent quantum confinement to achieve hot-carrier extraction and multiple exciton generation; however, their practical application faces challenges from surface-state-mediated recombination and ligand exchange complexities [32]. Nonetheless, challenges in interfacial engineering for tandem devices, particularly related to lattice mismatch and energy level alignment, demand atomic-level precision in heterojunction design. From a manufacturing point of view, moving from spin-coated lab-scale devices to industrial-scale processes like slot-die or vapor deposition introduces new complexities in crystallization control and defect management. Environmental concerns centered on lead content in perovskites and indium use in transparent electrodes have driven research into sustainable alternatives, such as Sn-based perovskites and carbon nanotube networks [33]. The future of third generation photovoltaics is increasingly focused on developing hybrid architectures that seamlessly combine the advantages of various different technologies, with ongoing research emphasizing the use of operando characterization techniques to better understand dynamic processes, leveraging machine

learning to accelerate the discovery of new, high performance materials, and implementing advanced light management strategies to maximize energy conversion efficiency toward thermodynamic limits, all while ensuring improved durability, scalability, and cost-effective fabrication processes to facilitate widespread commercial adoption and practical implement of these next-generation solar energy solutions.

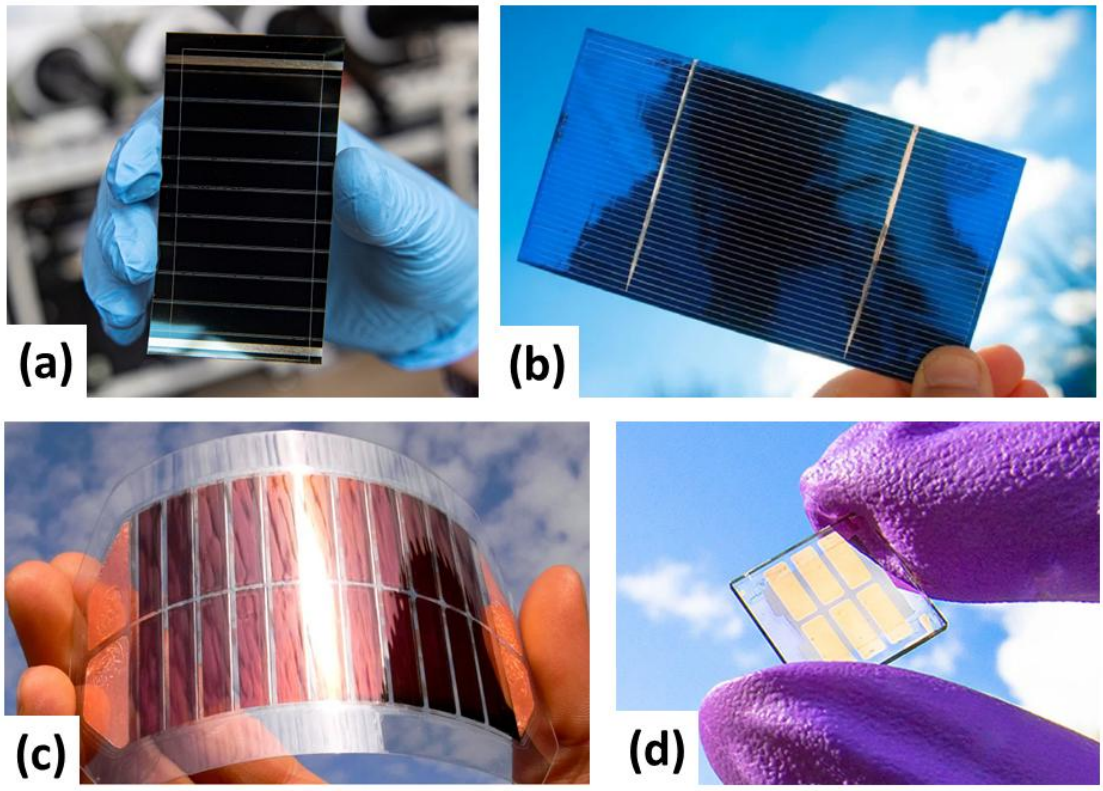

Fig 6. (a) Perovskite Solar Cell [34]**, (b) Dye Sensitized Solar Cell** [35]**, (c) Organic Solar Cell** [36]**, (d) Quantum Dot Solar Cell** [37]**.**

1.4.4 Fourth Generation of Solar Cells

Fourth-generation solar cells represent a transformative step in photovoltaic technology, integrating advanced nanomaterials, hybrid architectures, and novel physical mechanisms to push efficiency beyond conventional limits while introducing multifunctional capabilities. These cells combine the strengths of perovskites, quantum dots, organic semiconductors, and plasmonic nanostructures in innovative configurations such as perovskite-perovskite tandems and hybrid quantum dot-perovskite systems, achieving efficiencies exceeding 30% in experimental setups [28]. Key breakthroughs include engineered 2D/3D perovskite heterostructures for enhanced stability [38], plasmonic light-

trapping for improved absorption [39], and bio-inspired designs mimicking natural photosynthesis [40]. Unlike previous generations, fourth-generation photovoltaics emphasize tunable properties such as transparency, flexibility, and self-healing potential, enabling applications in building-integrated systems and wearable electronics. However, challenges in scalable fabrication, interfacial degradation, and material toxicity require further development of lead-free alternatives and AI-optimized manufacturing. With their very high efficiency potential and adaptability, fourth-generation solar cells are poised to redefine the future of renewable energy technologies.

1.5 Perovskite Solar Cells

Perovskite solar cells (PSCs) have originated as a revolutionary photovoltaic technology because of their unmatched optoelectronic properties, including low-temp solution processability, tunable bandgaps, high absorption coefficients, and long diffusion lengths. A longer diffusion length in a solar cell is crucial because it enables photogenerated charge carriers electrons and holes to travel greater distances before recombining. This increases the likelihood that these carriers will reach the p-n junction or electrodes to adds to electrical current, enhancing charge collection efficiency. Consequently, more energy is harvested from the absorbed light, boosting the cell's power output. Additionally, a longer diffusion length allows for the effective utilization of light absorbed deeper within the cell, especially from longer wavelengths, and helps the design of thinner, more efficient solar cells without compromising performance [41]. Overall, it is a primary element in maximizing the efficiency and effectiveness of solar energy conversion. First ever Perovskite solar cell was manufactured in 2009 with PCE of 3.8% [42] and PSCs have shown very rapid progress in efficiency in last 15 years and has attained highest efficiency of about 27% [28]

1.5.1 History of Perovskite Solar Cells

German mineralogist Gustav Rose made the initial discovery of perovskite materials in 1839 when he isolated the mineral calcium titanate ($CaTiO_3$) in the Russian Ural Mountains [43]. He gave the substance the name "perovskite" in reference to Lev Perovski, a Russian mineralogist. Later, a complete class of minerals with a similar crystal structure were named after this mineral. Caesium lead halide perovskite materials, which would later be essential in solar applications, were created in the lab by scientists by 1892 [44].

By 1945, X-ray crystallography had verified the theoretically generated perovskite crystal structure in minerals such as barium titanate, which had been known since 1926 [45].

Perovskite materials were first used in solar technology somewhat later. Research on their potential for photovoltaic applications began to pick up steam in 2006. When Japanese researchers Tsutomu Miyasaka and associates published the first PSC in 2009, with a power conversion efficiency of 3.8%, it was a significant turning point [42]. This was the start of a quick and amazing voyage. By 2011, scientists had fixed certain stability problems and increased efficiency to 6.5% [46]. The substitution of a solid-state hole transport material (spiro-OMeTAD) for the liquid electrolyte by Henry Snaith and Mike Lee in 2012 marked a substantial advancement in stability and increased the PCE to 10% [46]. From 2013, efficiency increased to 12–15% thanks to contributions from both mesoporous and planar device designs [47]. Perovskite solar cells are a severe competitor to conventional Si PV cells, with an astonishing 21% efficiency by 2015 [48]. A significant step towards commercialisation was taken in 2017 when researchers not only proved devices that could function steadily for a whole year under continuous illumination, but also achieved even better efficiency of 22.7% [49]. The trend persisted until 2020, when approved single-junction perovskite solar cells outperformed traditional silicon solar cells with an efficiency of 25.2% and tandem perovskite-silicon devices with an efficiency of 29.1% [50]. By 2024 , highest efficiencies of Perovskite Solar Cells is 27% , for Perovskite tandem solar cell it is 30.1% and for Perovskite/Si Hybrid tandem it is 34.6 % as per 2024 efficiency report published by NREL [28]. Commercial interest had risen sharply by now, businesses from all around the world have started making investments in the big scale manufacturing of tandem Si-PSC.

Even with remarkable advancements, research is still ongoing in areas like scalable production techniques and long-term material stability. Because of their high efficiency, adjustable characteristics, and inexpensive manufacturing processes, PSCs are currently regarded as one of the most encouraging next-gen solar technologies. To get this technology into broad commercial use, researchers are now working to overcome the last obstacles, which are mostly related to gadget longevity and environmental resistance.

1.5.2 Perovskite Structure

The term perovskite structure describes a group of minerals that have a crystal structure alike to that of calcium titanate ($CaTiO_3$), mineral named for Russian mineralogist Lev Perovski and initially found in the Ural Mountains [51]. Since then, it has become a key structural paradigm in materials research, especially in the fields of electronics, solid-state physics, photovoltaics, and catalysis. The idealized perovskite structure is represented by the general formula ABX_3.

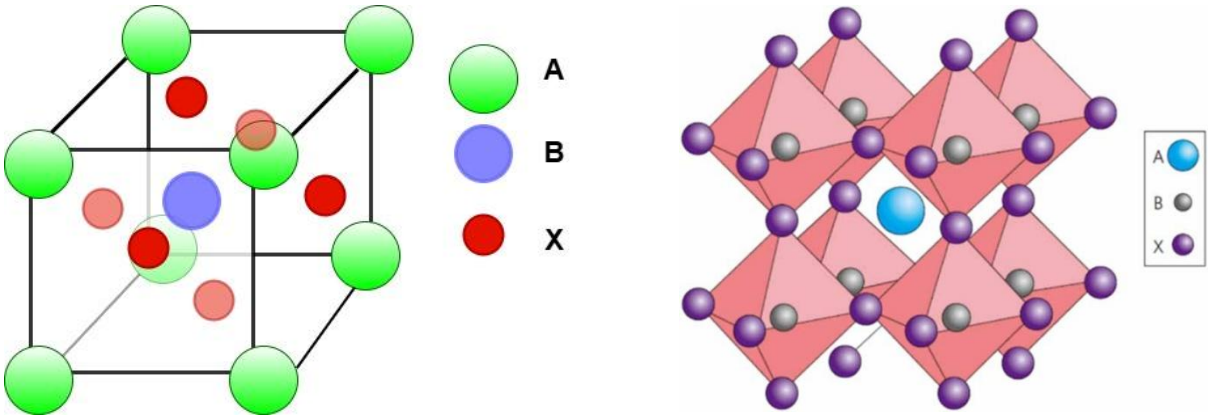

Fig 7. (a) Cubic cell structure of Perovskite material and **(b)** crystallographic structure of Perovskite material [52]

The perovskite lattice has three distinct types of ions: a larger A-site cation, a smaller B-site cation, and an X-site anion. The A-site cation, typically a rare-earth or alkaline-earth metal like calcium (Ca^{2+}), strontium (Sr^{2+}), or barium (Ba^{2+}), can also be an organic moiety like methylammonium ($CH_3NH_3^+$) in the case of hybrid perovskites. The B-site cation is a smaller transition metal ion such as titanium (Ti^{4+}), iron (Fe^{3+}), lead (Pb^{2+}), or tin (Sn^{4+}). The X-site anion is generally either a halide (e.g., iodide, bromide, chloride) in halide perovskites or oxygen in the case of oxide perovskites [53].

The B-site cation in the cubic cell is situated at the centre of the body, which is the centre of the cube. Six X anions, which are placed at the centre of each face of the cube, coordinate it octahedrally. The material's structural backbone is defined by the corner-sharing BX_6 octahedra that these anions produce in three dimensions. The A-site cation, which is significantly larger than the B-site cation, resides on eight corners of cube. Each A-site cation is enclosed by twelve X anions, forming a cuboctahedral coordination

environment [54]. A large variety of ionic sizes and combinations can be effectively accommodated by the structure thanks to its straightforward cubic geometry. Very high structural flexibility is conferred by the symmetry and packing arrangement that result, allowing for the substitution of a vast set of elements at the A, B, or X positions without sacrificing the overall lattice framework.

The expression of Goldschmidt tolerance factor (t) equation is:

$$t = \frac{r_A + r_X}{\sqrt{2}(r_B + r_X)} \quad (1)$$

Where r_A shows ionic radius of the A-site cation, r_B shows ionic radius of the B-site cation, t represents Goldschmidt tolerance factor, and r_X is the ionic radius of the anion (usually a halide or O^{2-}). $t \approx 1$ corresponds to an ideal cubic structure, $0.9 < t < 1.0$ typically leads to slightly distorted orthorhombic or tetragonal phases and $t < 0.9$ may result in significant octahedral tilting and the formation of lower-symmetry structures [55].

The physical characteristics of the material are significantly impacted by these aberrations. Ferroelectricity, magnetoresistance, superconductivity, and remarkable photovoltaic behaviour are only a few of the many functionalities made possible by the structural plasticity of perovskites, which permit broad chemical replacement at all three locations. Specifically, hybrid organic-inorganic halide perovskites have transformed the solar energy industry by providing low-cost solution processing and excellent power conversion efficiencies. In order to design and develop next-generation electrical, optoelectronic, and energy materials, the perovskite structure remains a fundamental theme.

1.5.3 Working Principle of Perovskite Solar Cells

A number of layers are commonly found in PSCs, and each layer is essential for the functioning of the device. An electron transport layer (ETL), such as titanium dioxide (TiO_2), which promotes electron mobility, comes after a transparent conductive substrate, such as FTO. At the centre of the device is the light-absorbing perovskite layer, which is inserted between HTL and ETL layer. A metal electrode is used to collect the holes after a HTL, is deposited above the perovskite layer [56]. High photovoltaic performance is made possible by this architecture's separation of charge effectively and collection capabilities. The operation of perovskite solar cells (PSCs) involves several key processes that contribute to their high efficiency in converting sunlight into electrical energy. When

light is assimilated by the perovskite layer, it generates electron-hole pairs, known as excitons. These excitons are then dissociated into free electrons and holes because of the preferable electronic properties of the material.

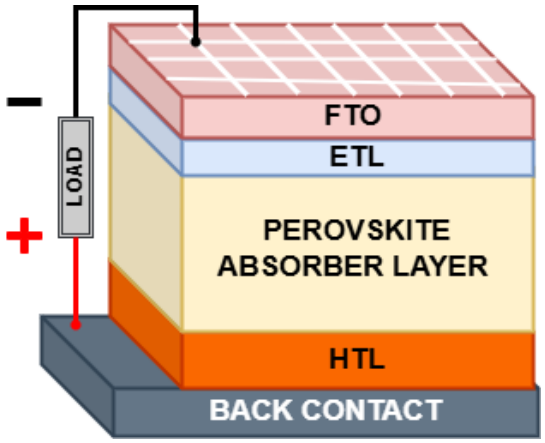

Fig 8. Device Architecture of Perovskite Solar Cells

An internal electric field, generally produced by a built-in potential between the ETL and HTL, propels the electrons and holes through the perovskite layer. While the HTL, which serves to minimize recombination of charge carriers, ensuring efficient extraction of holes, and helps maintain the in total stability and performance of the PV cell. The ETL, which have high electron mobility and is finely aligned with the CB of the light-absorbing layer. The ETL helps to prevent the recombination of charge carriers and ensures that electrons are efficiently transferred to the electrode, contributing to the overall performance and stability of the solar cell. Both the electrons and the holes are moved to the ETL and HTL, respectively [57]. After the electrodes have gathered these charge carriers, an electrical current that can be employed as power is produced. The superior light absorption properties and effective charge transfer of the perovskite material, which reduce energy loss during cell operation, contribute to this extremely effective process.

Most of the recently reported articles with efficiently performing $FASnI_3$ solar cells have used HTL like PEDOT: PSS and Spiro-OMeTAD. Though these HTLs give good results but they are organic in nature and they lack in many features like thermal stability, stability under ambient condition, chemical compatibility and limited intrinsic hole transport property [58]. PEDOT: PSS is acidic and hygroscopic (absorbs water from air), which can degrade the perovskite layer and reduce the device lifespan. Spiro-OMeTAD requires additives like Li-TFSI (Lithium bis(trifluoromethanesulfonyl)imide) and tBP (tert-

Butylpyridine) for improved conductivity[59] , which absorb moisture and lead to long-term degradation. That is why there is a need to explore and study more materials like CBTS that can be used for HTL layer.

CHAPTER 2:
LITERATURE SURVEY

CHAPTER 2: LITERATURE SURVEY

2.1 First Ever Perovskite Solar Cell and Early Developments

Kojima et al. [60] in 2009 in their pioneering publication, introduced a novel application of organometal halide perovskites as visible-light sensitizers for photovoltaic devices, specifically within dye-sensitized solar cells (DSSCs). They prepared $CH_3NH_3PbI_3$ (methylammonium lead iodide) and methylammonium $CH_3NH_3PbBr_3$(lead bromide), both of which feature a perovskite crystal structure renowned for their strong visible-spectrum absorption. These materials revealed excellent compatibility with mesoporous titanium dioxide (TiO_2) films, serving as the electron-transporting layer. Incorporating these perovskites into liquid-electrolyte-based DSSCs, the researchers achieved power conversion efficiencies up to 3.8%, a significant milestone at the time given the novelty of using organometal halide perovskites in this context.

This study showed that perovskites could serve as highly effective light harvesters, thanks to their exceptional absorption coefficients and favourable band alignment for efficient charge injection into TiO_2. However, the researchers noted that device effectivity declined swiftly over time because of the dissolution of perovskite materials in liquid electrolytes, underscoring stability as a major challenge for future development. Despite of this limitation, the work was groundbreaking as it was the first one to introduce the concept of using organometal halide perovskites in solar energy conversion, a breakthrough that soon revolutionized photovoltaics. The findings provided the scientific community with a new class of promising materials and initiated a increase of research aimed at enhancing both efficiency and stability through the development of solid-state device architectures in subsequent years.

Jeong-Hyeok Im et al. [61] in 2011 showed a significant breakthrough in perovskite solar cell development. In this work, the researchers used methylammonium $CH_3NH_3PbI_3$ (lead iodide) as the photosensitive material within a dye-sensitized PV cell (DSSC) architecture, but with an innovative approach: employing perovskite materials in quantum dot form. This strategy enhanced light absorption and charge transport, ultimately improving the device's efficiency and opening new avenues for perovskite solar technologies. The researchers enhanced the stability and photovoltaic performance of perovskite layers, achieving a PCE of 6.5%, up from around 3.8% in 2009. They optimized the precursor

solution's concentration and deposition, ensuring better coverage and minimizing recombination. However, devices still used liquid electrolytes and remained moisture-sensitive, leading to stability issues. Nonetheless, this work marked a key step in demonstrating higher efficiencies and highlighting the need for more stable, solid-state architectures, paving the way for future advancements.

Lee et al. [62] made a significant advancement in perovskite solar cell design in their groundbreaking 2012 paper. They were able to successfully develop a solid-state device architecture that substituted a solid-state hole transport material (HTM), specifically spiro-OMeTAD, for the conventional liquid electrolyte. The researchers synthesized a meso-superstructure solar cell with exceptional efficiency and enhanced stability by embedding the light-absorbing layer of the organometal halide perovskite $CH_3NH_3PbI_3$ in a mesoporous alumina scaffold (Al_2O_3). With a PCE of 10.9%, this innovative design roughly tripled the performance of previous liquid electrolyte-based perovskite-based devices.

Using spiro-OMeTAD facilitated efficient hole extraction and transport, overcoming the critical issue of perovskite dissolution that hindered earlier designs. Additionally, the alumina scaffold's insulating properties showed that electron conduction could occur directly from the perovskite absorber to the compact TiO_2 layer, challenging previous beliefs about the necessity of mesoporous structures. This work signified a pivotal step toward fully solid-state perovskite solar cells and is widely recognized as a foundational study that catalysed rapid advancements and global interest in perovskite photovoltaic research

Lee et al. [62] made a significant advancement in perovskite solar cell design in their groundbreaking 2012 paper. They were able to successfully develop a solid-state device architecture that substituted a solid-state hole transport material (HTM), specifically spiro-OMeTAD, for the conventional liquid electrolyte. The researchers created a meso-superstructure solar cell with exceptional efficiency and improved stability by embedding the light-absorbing layer of the organometal halide perovskite $CH_3NH_3PbI_3$ in a mesoporous alumina scaffold (Al_2O_3). With a power conversion efficiency (PCE) of 10.9%, this innovative architecture roughly tripled the performance of previous liquid electrolyte-based perovskite-based devices.

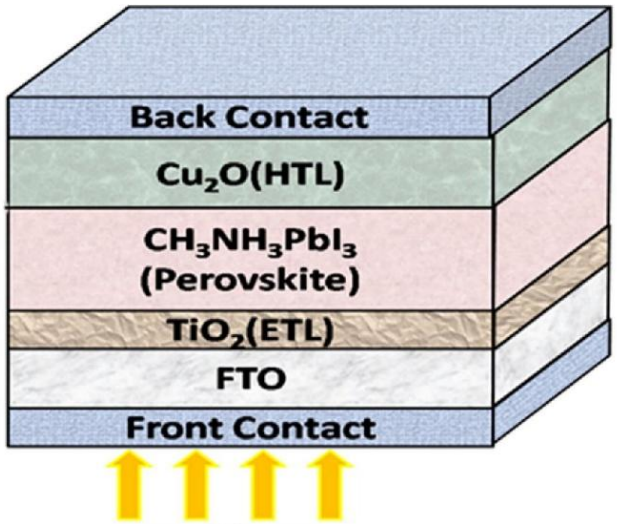

Fig 9. $CH_3NH_3PbI_3$ perovskite Solar Cell

2.2 Lead-free Perovskite Solar Cells

In section 2.1, it is evident that early absorber perovskite materials used in PSCs were Lead based and it is observed that these solar cells could be harmful for the environment after the degradation. Hence, there was need to replace Pb based perovskites with some environmentally friendly perovskite material.

Peidong Su et al. [63] in study tests the environmental risks posed by disposing of lead-based perovskite solar cells (PSCs). Utilizing dynamic leaching tests (DLTs) with fluids like TCLP, SPLP, and deionized water mimicking landfill conditions, acid rain, and natural water exposure the researchers quantified the release of heavy metals and organic pollutants from discarded PSCs. Results showed substantial lead leaching, especially under SPLP conditions, with lead concentrations reaching 5.585 mg/L above the U.S. EPA hazardous waste limit of 5.0 mg/L. Increased levels of TOC (total organic carbon) and COD (chemical oxygen demand) indicated significant organic contaminant release, highlighting ecological and atmospheric pollution concerns linked to PSC disposal. Microscopic (SEM) and crystallographic (XRD) analyses showed that the active layers of PSCs degrade structurally upon environmental exposure, leaving primarily the fluorine-doped tin oxide (FTO) glass substrate intact. These results revealed the vulnerability of PSC materials to decomposition and the potential release of contaminants in disposal scenarios. The study concludes that improperly managed discarded lead-based PSCs pose a significant environmental risk due to leaching of toxic metals and organic residues. It signifies the need for effective recycling methods, safer encapsulation techniques, and the

development of environmentally friendly, lead-free alternatives, alongside stricter regulations to prevent long-term ecological contamination.

Fabini et al. [64] in their insightful viewpoint article, examine the environmental implications of widespread deployment of lead-halide PSCs in the United States. Using crystal structure data for $CH_3NH_3PbI_3$, typical device configurations, and optimistic photovoltaic performance assumptions (25% efficiency, 25-year lifespan, 20% capacity factor), they estimate a lead intensity of approximately 38 μg per kWh. To meet the whole U.S. electricity demand, roughly 160 metric tons of lead would be required annually. If just 1% of these modules fail over time, this could release about 1.6 tons of lead annually into the environment. The authors compare these figures with historical and current lead emissions from sources such as coal burning, electronic solder, and leaded gasoline, highlighting the potential environmental impact of large-scale perovskite PV deployment.

The study highlights that, although the lead in PSCs is contained within solid, encapsulated structures unlike the airborne emissions historically associated with leaded gasoline there remains a detectable environmental risk, particularly if devices are damaged or improperly disposed of. Fabini emphasizes that, while the total lead quantities from PSCs are relatively small compared to legacy sources, implementing rigorous encapsulation, establishing proper disposal protocols, and conducting further research into degradation and leaching behaviours are crucial for the safe commercialization of this technology. Overall, the paper demonstrates the importance of evaluating all environmental trade-offs when developing and deploying new photovoltaic materials.

Hao et al. [65] in 2014 published a groundbreaking study in introducing the first Pb-free PSC, dealing with the toxicity related issues with traditional Pb-based perovskites. They replaced lead with tin (Sn), particularly using methylammonium tin iodide ($CH_3NH_3SnI_3$) as the active light-absorbing material. This new compound retained key optical properties of perovskites, such as a direct bandgap of around 1.3 eV and strong light absorption capabilities. Although the instability of Sn^{2+} which easily oxidizes to Sn^{4+} posed significant challenges, the fabricated PV cell gained a η of 5.73%, revealing the potential of lead-free alternatives. This pioneering work not only opened new avenues for environmentally friendly perovskite materials but also laid a foundation for ongoing research aimed at

optimizing tin-based and other non-toxic perovskite compositions for sustainable solar energy solutions.

Liping Peng et al. [66] in the paper analyse the BPVE (Bulk Photovoltaic Effect) in tin-based, Pb-free perovskites. Combining theoretical calculations and experimental results, the study examines these materials as eco-friendly alternatives to lead-based perovskite solar cells. The authors analyse key intrinsic properties, including electronic structure and band gap, to find their potential for efficient photocurrent generation via BPVE. Findings reveal that $FASnI_3$ shows superior optical and electronic characteristics compared to $MASnI_3$, positioning it as a more promising candidate for high-efficiency, lead-free solar devices.

The researchers employed computational methods to model the electronic structures of $MASnI_3$ and $FASnI_3$, revealing that $FASnI_3$'s narrower band gap and improved charge transport are key factors behind its superior performance. Experimental validation corroborated these results, with $FASnI_3$-based solar cells showing higher power conversion efficiencies than those using $MASnI_3$. Overall, the study highlights $FASnI_3$'s promising potential as a lead-free perovskite material, paving the path for environmentally friendly and efficient photovoltaic technologies.

2.3 Study of Different HTLs and ETLs used in Perovskite Solar Cells

Hossain et al. [67] did a simulation study using SCAPS-1D to explore how different ETLs and HTLs influence the effectiveness of all-inorganic $CsPbI_3$-based perovskite solar cells. They tested various ETLs—such as TiO_2, ZnO, SnO_2, and PCBM-and HTLs-including CuI, CuSCN, CBTS, PEDOT: PSS, and Spiro-OMeTAD to assess their impact on key photovoltaic metrics: J_{SC} (short-circuit current), V_{OC} (open-circuit voltage) , FF (fill factor), and η% . The model was also validated with experimental data to promise accuracy.

Results demonstrated that the combination of TiO_2 as the ETL and Spiro-OMeTAD as the HTL delivered the best performance, achieving a PCE of 17.10%, Voc of 1.10 V, Jsc of 20.62 mA/cm², and FF of 75.11%. The study signifies the importance of energy level alignment, carrier mobility, and defect density in transport layers, which critically influence device efficiency. These results highlight that careful selection of ETL and HTL materials can notably improve the stability and η of $CsPbI_3$-based perovskite solar cells,

providing valuable insights for future experimental development of more efficient and durable perovskite photovoltaics.

G. F. Ishraque Toki et al. [68] conducted an extensive study on lead-free $CsSnCl_3$-based PSCs using SCAPS-1D simulations and DFT (density functional theory) calculations. The researchers examined 96 different configurations of ETLs and HTLs to optimize the device effectivity. Their simulations revealed that ETLs like TiO_2, ZnO, and IGZO, combined with CBTS as the HTL, achieved the highest power conversion efficiency (PCE) of up to 22%. The study also explored the impact of absorber and ETL thickness, series and shunt resistance, temperature, and other factors on cell performance. Additionally, DFT calculations gave insights into the structural, electronic, and optical properties of $CsSnCl_3$, confirming its suitability as a solar absorber due to its direct bandgap and favourable charge transport characteristics. The results were further validated using wxAMPS simulations, ensuring the reliability of the findings.

The optimized device structure, ITO/TiO_2/$CsSnCl_3$/CBTS/Au, demonstrated outstanding performance with a PCE of 21.75%, VOC of 1.01 V, JSC of 26.22 mA/cm², and FF of 82.03%. The study also emphasized the importance of band alignment, thickness optimization, and defect reduction in achieving high-performance PSCs. By combining theoretical simulations with experimental validation, the work demonstrates a comprehensive guide for fabricating cost-effective and efficient lead-free perovskite solar cells, contributing to sustainable energy solutions.

CHAPTER 3:

INTRODUCTION TO SCAPS SIMULATION AND DEVICE SIMULATION METHODOLOGY

CHAPTER 3: INTRODUCTION TO SCAPS SIMULATION AND DEVICE SIMULATION METHODOLOGY

3.1 Introduction to SCAPS 1D Simulation

SCAPS (Solar Cell Capacitance Simulator) is a one-dimensional simulation software developed by the University of Ghent, Belgium, for analysing thin-film solar cells. It models electrical characteristics by defining material layers, their properties, and interfaces, solving Poisson's and continuity equations for electrons and holes to simulate I-V, C-V, and quantum efficiency. Supporting materials like perovskites, CIGS, and CdTe, users can input parameters such as bandgap, doping, defect levels, and layer thickness. SCAPS is widely used in research for device optimization before fabrication, thanks to its user-friendly interface and powerful simulation capabilities. Also, it comes out to be very accurate when simulated studies are compare to the experimental works.

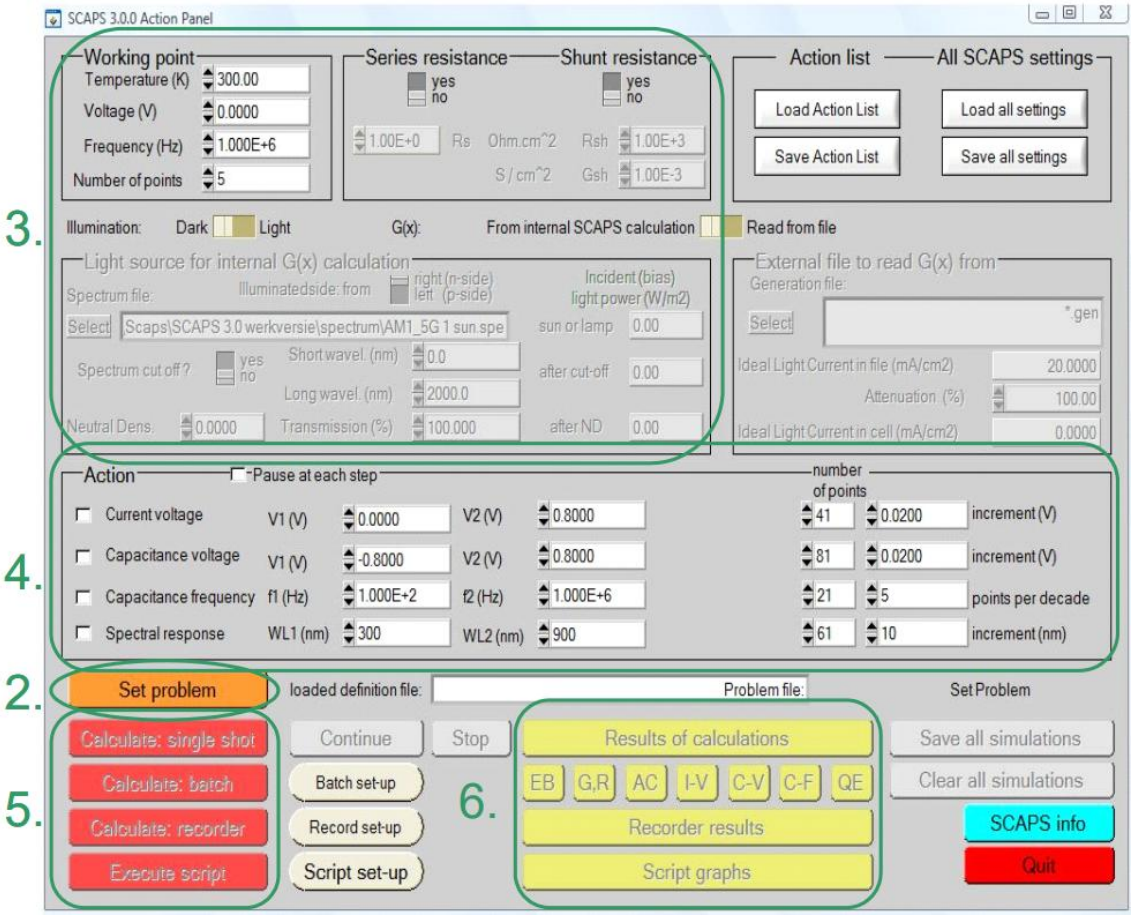

Fig 10. Front Panel of SCAPS 1D software [69].

The SCAPS Start-Up Panel guides users through the simulation process in six organized panels. Panel 1 launches SCAPS and opens the main interface; Panel 2 involves defining the device structure, including layers, materials (like ZnO, CdS, CIGS), and properties such as bandgap, doping, defects, and thickness. Panel 3 sets the working conditions, specifying illumination (e.g., AM 1.5), temperature, and bias voltage. Panel 4 allows selection of the desired calculations - I-V, C-V, QE, etc. After inputting these parameters, Panel 5 initiates the simulation, where SCAPS solves the physical equations to model device behaviour. Finally, Panel 6 displays the results via graphs and curves, such as I-V characteristics or energy band diagrams. This structured workflow ensures an intuitive and efficient process for solar cell analysis and optimization.

3.2 Device Structure

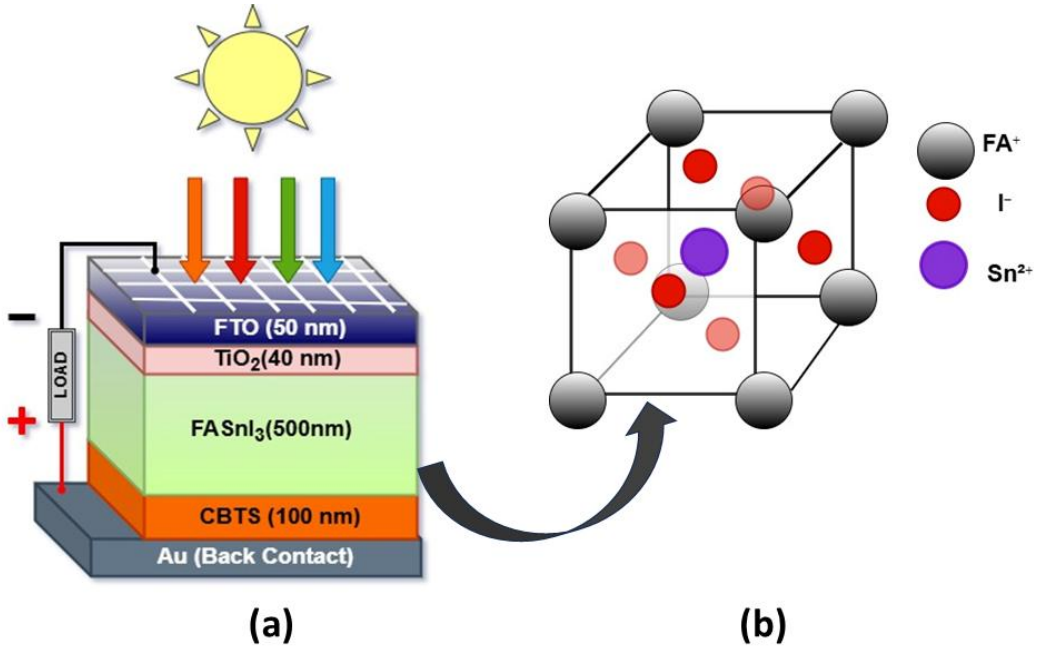

Figure 11. (a) Schematic diagram of the suggested perovskite PV cell with CBTS as HTL and **(b)** Unit cell structure of $FASnI_3$.

In Figure 11(a) we can see the schematic diagram of the simulated structure of perovskite photovoltaic solar cell. Each constituent layer of the solar cell plays a critical role in determining its overall efficiency. The ETL and hole HTL not only facilitate charge carrier transport but also establish an internal electric field due to their intrinsic n-type and p-type doping characteristics. This built-in field is essential for directing charge carriers toward their respective electrodes via drift mechanisms. The perovskite absorber layer performs

multiple critical functions integral to device operation. It efficiently harvests incident photons, generating photogenerated charge carriers, facilitates their dissociation into free e^- and h^+, and directs their initial transport towards the electron transport layer (ETL) and hole transport layer (HTL) to enable charge separation and collection processes[70]. $FASnI_3$ is used as Lead free absorber layer, Copper Barium Tin Sulphide (CBTS) is taken as HTL and TiO_2 is taken as ETL. Gold (Au) and Aluminium (Al) are taken as back and front contact respectively. Fig 11(b) shows the unit cell structure of $FASnI_3$. Formamidinium tin iodide ($FASnI_3$) is a halide perovskite with an ABX_3 structure, where A = FA^+ (Formamidinium), B = Sn^{2+} (Tin), and X = I^- (Iodide). At room temperature, it crystallizes in a cubic perovskite structure, with Sn^{2+} on the centre of the unit cell, I^- ions at the face-centred positions, and FA^+ at the corners occupying the cubic voids between the corner-sharing SnI_6 octahedra [71].

3.3 Simulation Methodology and Optimisation of Input Parameters

The device is simulated using the SCAPS (3.3.09) solar cell simulation program, which is highly regarded by solar cell experts for its accuracy in aligning simulated outcomes with real-world results and prior global research. The physics of device simulation in SCAPS-1D is governed by the numerical solution of one-dimensional semiconductor equations, which encompass Poisson's equation, continuity equations, and carrier transport equations while accounting for various recombination mechanisms. By solving these coupled differential equations for a defined device structure, SCAPS-1D enables the computation of key photovoltaic performance parameters [72]. Poisson's equation for e^- and h^+ is represented by:

$$\frac{d}{dx}\left(\epsilon\frac{d\psi}{dx}\right) = -\frac{q}{\epsilon}(p - n + N_D^+ - N_A^- + \rho_t) \quad (2)$$

Where ε refers to permittivity of the material, ψ refers to electrostatic potential, q is elementary charge, p and n refer to hole and electron concentrations respectively, N_D^+ and N_A^- refer to ionized donor and acceptor densities, and ρ_t refers to charge density due to traps.

Continuity equations are given by:

$$\frac{dJ_n}{dx} + qG - qR = 0 \quad (3)$$

$$\frac{dJ_p}{dx} - qG + qR = 0 \quad (4)$$

Where J_n and J_p refers to electron current density and hole current density respectively, G refers to electron-hole pair generation rate, and R refers to recombination rate.

Carrier transport equations are given by:

$$J_n = qn\mu_n E + qD_n \frac{dn}{dx} \quad (5)$$

$$J_p = qp\mu_p E - qD_p \frac{dp}{dx} \quad (6)$$

Where J_n and J_p refers to electron current density and hole current density respectively, E is electric field, D_n and D_p are electron and hole diffusion coefficient respectively, μ_n and μ_p are electron and hole mobility respectively.

SCAPS-1D also incorporates multiple recombination models like:

(a) Shockley-Read-Hall (SRH) Recombination (Trap-assisted)

$$R_{SRH} = \frac{np - n_i^2}{\tau_n(p+p_t)+\tau_p(n+n_t)} \quad (7)$$

Where τ_n and τ_p are electron and hole lifetimes and p_t, n_t are trap densities.

(b) Radiative Recombination (Band-to-band)

$$R_{\text{rad}} = B(np - n_i^2) \quad (8)$$

where B is the radiative recombination coefficient.

(c) Auger Recombination

$$R_{\text{Auger}} = C_n n(np - n_i^2) + C_p p(np - n_i^2) \quad (9)$$

where C_n, C_p are Auger recombination coefficients.

Also, open circuit voltage and short circuit current are given by:

$$V_{oc} = \frac{kT}{q} \ln\left(\frac{J_{ph}}{J_0} + 1\right) \quad (10)$$

$$J_{sc} = q \int_0^{\infty} \eta(\lambda)\Phi(\lambda)d \quad (11)$$

V_{OC} is to open-circuit voltage, k refers to the Boltzmann constant, T is absolute temperature (in Kelvin), q is the elementary charge, J_{ph} is photo current density, and J_0 refers to reverse saturation current density, $\eta(\lambda)$ refers to external quantum efficiency (EQE) at wavelength λ and $\Phi(\lambda)$ refers to incident photon flux at wavelength λ. SCAPS-1D solves differential equations (1)-(5) using the input values in Table 1 to determine the electrostatic potential and quasi-Fermi levels of holes & electrons in the solar cell under AM 1.5G illumination at 300 K.

Table 1 shows the optimised SCAPS parameters for different components of the device including HTL, ETL, absorber layer, different interfaces and metal contacts.

Table 1. Optimised SCAPS parameter.

Parameter	**CBTS** [68]	**$FASnI_3$** [73]	**TiO_2** [74]	**FTO** [73]
t (μm)	0.1	0.5	0.04	0.05
E_g (eV)	1.9	1.4	3.2	3.5
χ (eV)	3.6	4	3.9	4
ε	5.4	8.2	9	9
CB effective DOS (cm^{-3})	2.2×10^{18}	1.0×10^{18}	2.0×10^{18}	2.0×10^{18}
VB effective DOS (cm^{-3})	1.8×10^{19}	1.0×10^{18}	1.8×10^{19}	1.8×10^{19}
Electron thermal velocity (cm/s)	1.0×10^{7}	1.0×10^{7}	1.0×10^{7}	1.0×10^{7}
Hole thermal velocity (cm/s)	1.0×10^{7}	1.0×10^{7}	1.0×10^{7}	1.0×10^{7}
μ_n (cm^2/Vs)	30	22	100	20
μ_h (cm^2/Vs)	10	22	25	10
N_D (cm^{-3})	-	-	1.0×10^{16}	1.0×10^{15}
N_A (cm^{-3})	1.0×10^{18}	7.0×10^{16}	-	-
N_t (cm^{-3})	1.0×10^{15}	1.0×10^{15}	1.0×10^{15}	1.0×10^{15}

Interface parameters		
Parameters (unit)	CBTS / FASnI3 interface	FASnI3 / TiO2 Interface
Defect type	Neutral	Neutral
Electron capture cross-section, σ_e (cm^2)	1×10^{-15}	1×10^{-19}
Hole capture cross-section, σ_p (cm^2)	1×10^{-16}	1×10^{-19}
Defect position above the highest E_V (eV)	0.6	0.6
Interface defect density (cm^{-2})	1×10^{12}	1×10^{11}
Working temperature (K)	300 - 400	

Electrode material		
Contact parameters	Front electrode	Back electrode
Φ (eV)	4.2 (Al)	5.2 (Au)
SRV of electrons (cm/s)	1.00×10^{7}	1×10^{7}
SRV of holes (cm/s)	1.00×10^{7}	1×10^{7}

CHAPTER 4: RESULT AND DISCUSSION

CHAPTER 4: RESULT AND DISCUSSION

4.1 Analysis of J-V characteristics

The J-V (Current Density-Voltage) curve is a fundamental graph used to evaluate the photovoltaic performance of solar cells. In figure 12 (a) J-V curve of the cell simulated with absorber layer thickness of 0.5µm gives the J_{SC} of 29.61 mA/cm^2, V_{OC} is 1.126 V and J_{MPP} and V_{MPP} comes out to be 27.03 mA/cm^3 and 0.986 V respectively where MPP denotes maximum power point. The maximum area under J-V curve represents fill factor (FF) of the device and in proposed device and it comes out to be 83.20 % which is desirable for fabrication of high efficiency solar cells[75]. The maximum power point (MPP) is determined by the largest area enclosed under the J-V curve, as highlighted by the red square box, representing the optimal operating condition for maximum power output in solar cells. Further agenda of the author is to test impact of absorber layer thickness on the J-V curve performance. Increasing thickness enhances light absorption, boosting the short-circuit current density (J_{SC}) and overall power conversion efficiency (PCE). However, excessive thickness can lead to increased recombination losses and reduced fill factor (FF), negatively impacting efficiency. Optimizing thickness ensures a balance between effective charge transport and minimized recombination [76]. In this study, the thickness of the absorber layer varied from 0.2 µm to 1.0 µm in steps of of 0.2 µm, while maintaining other device parameters constant. For thinner absorber layers, a considerable fraction of incident light remains unabsorbed, resulting in reduced electron-hole pair generation and lower short-circuit current density (J_{SC}). As the thickness increases, enhanced light absorption facilitates greater charge carrier generation, leading to improved J_{SC}. However, beyond a critical thickness range of approximately 0.8-1.0 µm, the majority of useful photons are absorbed within the first few micrometres of the material. Further increase in thickness contribute minimally to charge generation and significantly elevate recombination losses. Excessive thickness also poses challenges for efficient carrier extraction, as deeper-generated carriers face higher recombination probabilities and diffusion limitations before reaching the junction [77]. However, once the thickness exceeds the carrier diffusion length, recombination dominates, and Jsc saturates[78]. As shown in Figure 12(d), varying absorber layer thickness does not affect V_{OC}. This is explained by Equation (10), where V_{OC} is determined by the logarithm of J_{ph}/J_0 (photocurrent density/reverse saturation

current density). For thick absorbers, this ratio remains relatively constant because J_{ph} and J_0 scale proportionally with thickness. Consequently, V_{OC} is primarily governed by the quasi Fermi level splitting at the junction, which depends on recombination and built-in potential, rather than absorber layer thickness [79].

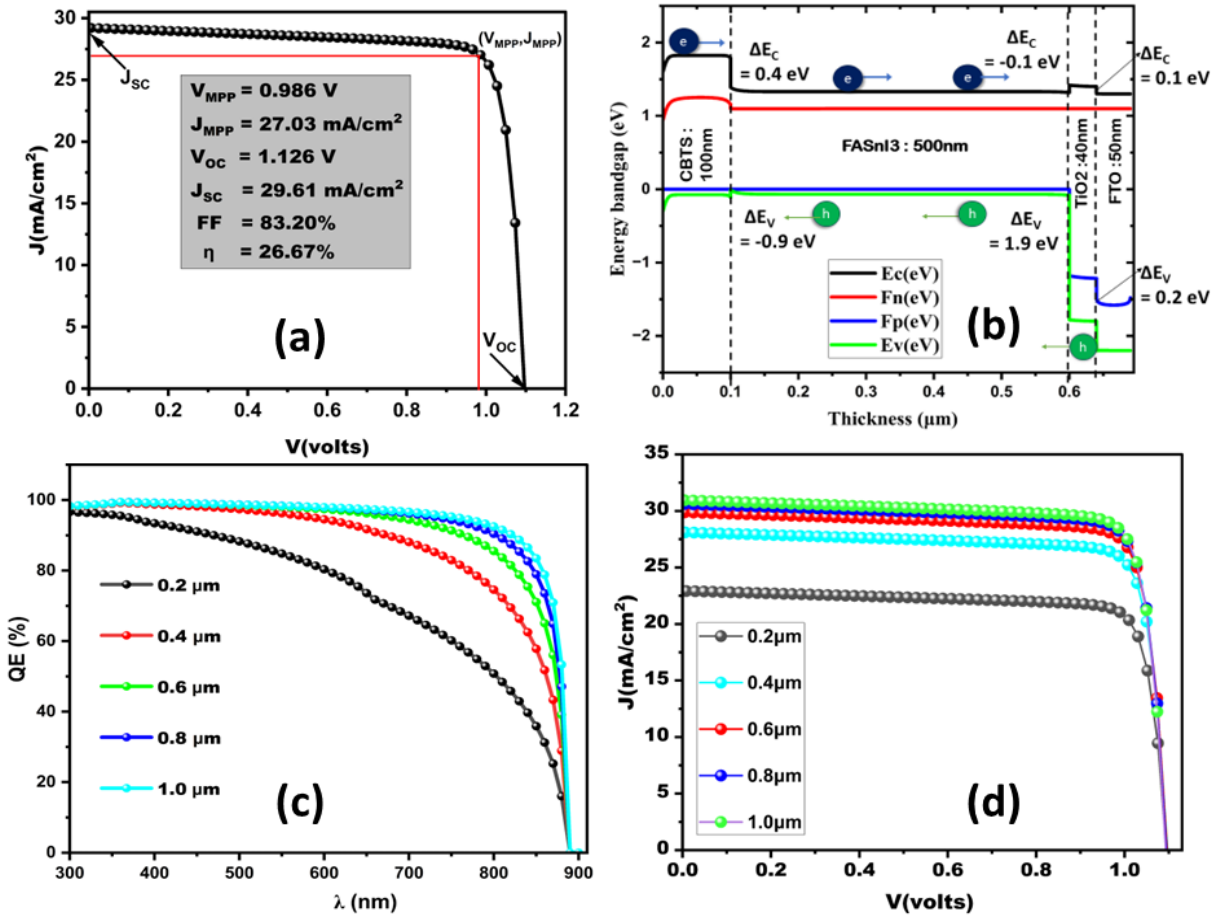

Fig 12. Analysis of **(a)** J-V characteristics **(b)** energy band diagram **(c)** absorber layer ($FASnI_3$) thickness on quantum efficiency and **(d)** effect of absorber layer thickness on J-V characteristics.

4.2 Quantum efficiency and band diagram analysis

Quantum efficiency (QE) in solar cells quantifies the fraction of incident photons that generate charge carriers contributing to current. Optical absorption governs photon capture, facilitating carrier generation, which in turn influences charge transport and recombination dynamics. Optimized material properties, effective passivation strategies, and precise interface engineering are essential to minimizing losses and enhancing device performance [80]. The solar cell's spectral response to incoming light is indicated by the variations in QE across different wavelengths. Figure 11(c) illustrates how quantum efficiency varies with different absorber layer thicknesses. In the simulation, the thickness

of the absorber layer is increased from 0.2 µm to 1.0 µm insteps of 0.2 µm keeping rest of the parameters remains same. A thicker absorber layer enables enhanced photon absorption, particularly for longer wavelengths that penetrate deeper into the material. Increased thickness promotes the generation of electron-hole pairs, resulting in higher charge carrier collection and improved quantum efficiency. However, beyond an optimal thickness threshold, quantum efficiency shows negligible improvement, as the majority of photons are already absorbed within this range. Excessive thickness further exacerbates recombination losses, as charge carriers generated at greater depths face increased recombination probabilities before reaching the electrodes. This interplay between photon absorption and recombination establishes a practical limit on the absorber layer thickness for achieving maximum quantum efficiency[81]. Figure 11(b) illustrates the energy band diagram, essential for analyzing charge carrier dynamics in solar cells. It provides insights into band alignment, transport mechanisms, and recombination pathways to optimize device performance. It reveals the alignment of conduction and valence bands, enabling efficient charge separation and transport. This diagram helps identify potential barriers at interfaces, minimizing recombination losses and enhancing efficiency. It provides insights into material properties, such as work function and bandgap, essential for designing advanced architectures. In the simulated device structure, three heterojunctions are formed namely CBTS/$FASnI_3$, $FASnI_3$/TiO_2, and TiO_2/FTO. The valence band offsets (VBO) for these heterojunctions are −0.9 eV, +1.9 eV, and +0.2 eV, respectively. Meanwhile, the conduction band offsets (CBO) are +0.4 eV, −0.1 eV, and +0.1 eV, respectively. The VBO and CBO for the $FASnI_3$/TiO_2 heterojunction is calculated by the equations (12) & (13) [82][83]:

$$CBO = \chi_{TiO_2} - \chi_{FASnI_3} \quad (12)$$

$$VBO = \left(E_{g\,TiO_2} - E_{g\,FASnI_3}\right) - \left(\chi_{TiO_2} - \chi_{FASnI_3}\right) \quad (13)$$

Where χ represents electron affinity and E_g represents band gap of the materials. Effective hole extraction in perovskite solar cells necessitates precise alignment between the valence band of the perovskite absorber $FASnI_3$ and the highest occupied molecular orbital (HOMO) of Cu_2BaSnS_4 (CBTS). This band alignment minimizes energy barriers, enhances charge transport, and reduces interfacial recombination, contributing to improved photovoltaic performance and device stability. Misalignment in this region can lead to suboptimal hole extraction, resulting in increased recombination and lower device

efficiency. The conduction band of $FASnI_3$ aligns with the LUMO (lowest unoccupied molecular orbital) of TiO_2 shown in figure 11 (b), promoting effective electron transport from the perovskite to the electron transport layer (ETL). Misalignment between the conduction band of the perovskite and the LUMO of the ETL can result to electron accumulation at the interface, causing charge recombination and reducing device performance. Proper band alignment is critical for efficient electron transport from the perovskite to the ETL, followed by the movement of electrons to the FTO substrate and through the external circuit to the front electrode[84].

4.3 Impact of work function

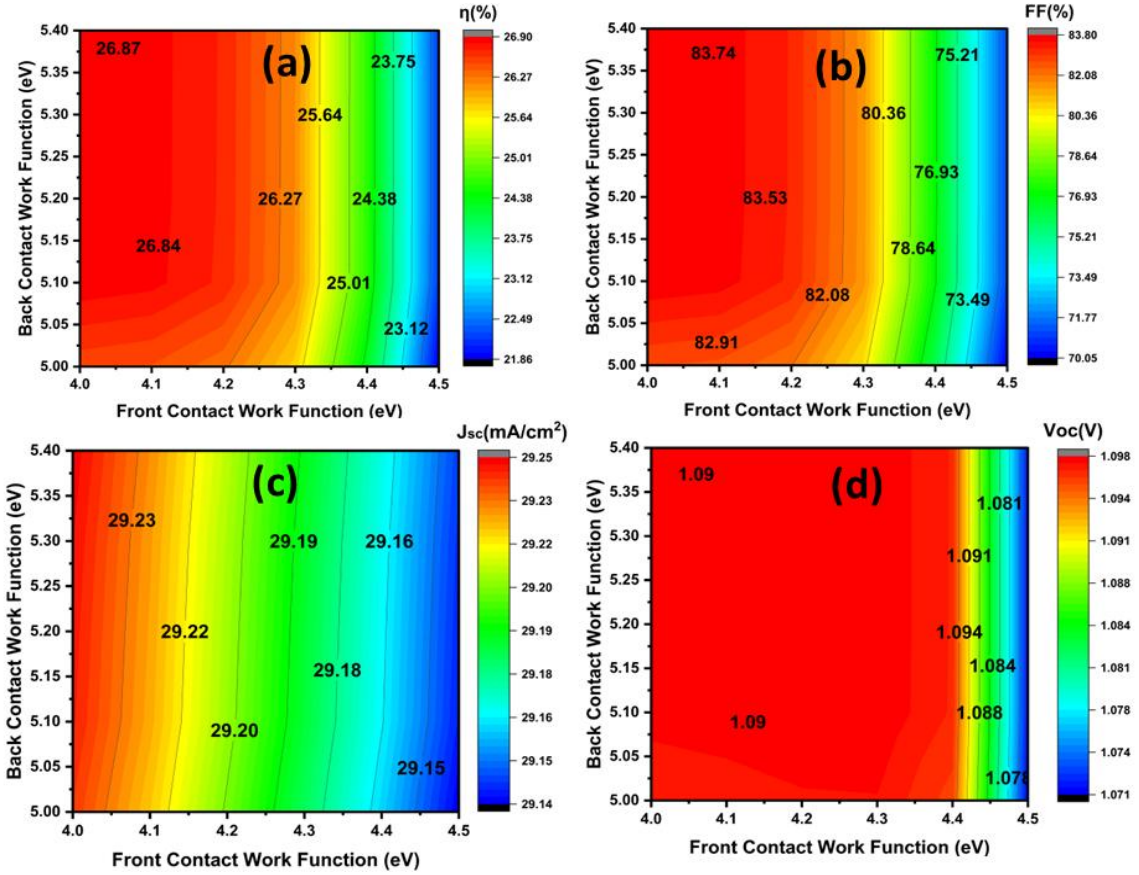

Fig 13. Contour mapping analysis of back and front contact work function on **(a)** efficiency **(b)** fill factor, **(c)** current density and **(d)** voltage.

The work function of photovoltaic materials directly influences charge transport efficiency, energy band alignment, and interfacial recombination dynamics[85]. Mismatched work functions can create energy barriers, increasing recombination and reducing device performance. Optimizing contact materials enhances V_{OC}, FF and overall η. To assess the ohmic behaviour of the proposed solar cell, Authors systematically varied the work functions of both the front and back metal contacts, as illustrated in figure 13.

The work function of the back contact adjusted within a range of 5.00 eV to 5.40 eV, while the front contact work function was modified between 4.00 eV and 4.50 eV. These adjustments significantly impacted photovoltaic performance, resulting in efficiency (η) variations from 21.86% to 26.90%, open-circuit voltage (V_{OC}) changes from 1.071 V to 1.098 V, fill factor (FF) enhancements from 70.05% to 83.80%, and fluctuations in short-circuit current density (J_{SC}) from 29.14 mA/cm² to 29.25 mA/cm², as shown in Figure 3. The optimal photovoltaic characteristics were achieved with a back contact work function of 5.2 eV and a front contact work function of 4.2 eV, utilizing copper bismuth telluride sulphide (CBTS) as the hole transport layer (HTL).Previous studies indicate that to attain high solar cell efficiency, it is essential for the back contact metal to have a work function exceeding 5 eV, with a minimum of 5.15 eV required to form ohmic or near-ohmic contacts in heterojunction photovoltaic structures[72]. This research confirms that employing a back contact work function of approximately 5.2 eV (Au) combined with a front contact work function of 4.2 eV (Al) is optimal for establishing efficient ohmic contact.

4.4 Effect of temperature and acceptor density

Temperature affects carrier mobility, recombination rates, and bandgap, influencing open-circuit voltage (V_{OC}) and overall efficiency. Higher acceptor density enhances charge collection but can increase recombination losses, impacting fill factor (FF) and short-circuit current density (J_{SC}). Optimizing both parameters is crucial for achieving stable and high-performance solar cells [86].

In figure 14 (a), when temperature increase from 300K to 400K results in a marginal shift in J_{SC} but a sharp reduction in V_{OC}, FF, and η. This trend is attributed to bandgap narrowing and the rise in reverse saturation current with temperature [87]. At higher thermal energies, enhanced carrier generation results to greater electron excitation from the VB to CB. However, increased carrier scattering and recombination rates reduce charge collection efficiency, thereby diminishing mobility and overall device performance[88].

According to Varshni's equation (14), the temperature dependence of the band gap energy of semiconductors is given by:

$$E_g(T) = E_g(0) - \frac{\alpha T^2}{T+\beta} \quad (14)$$

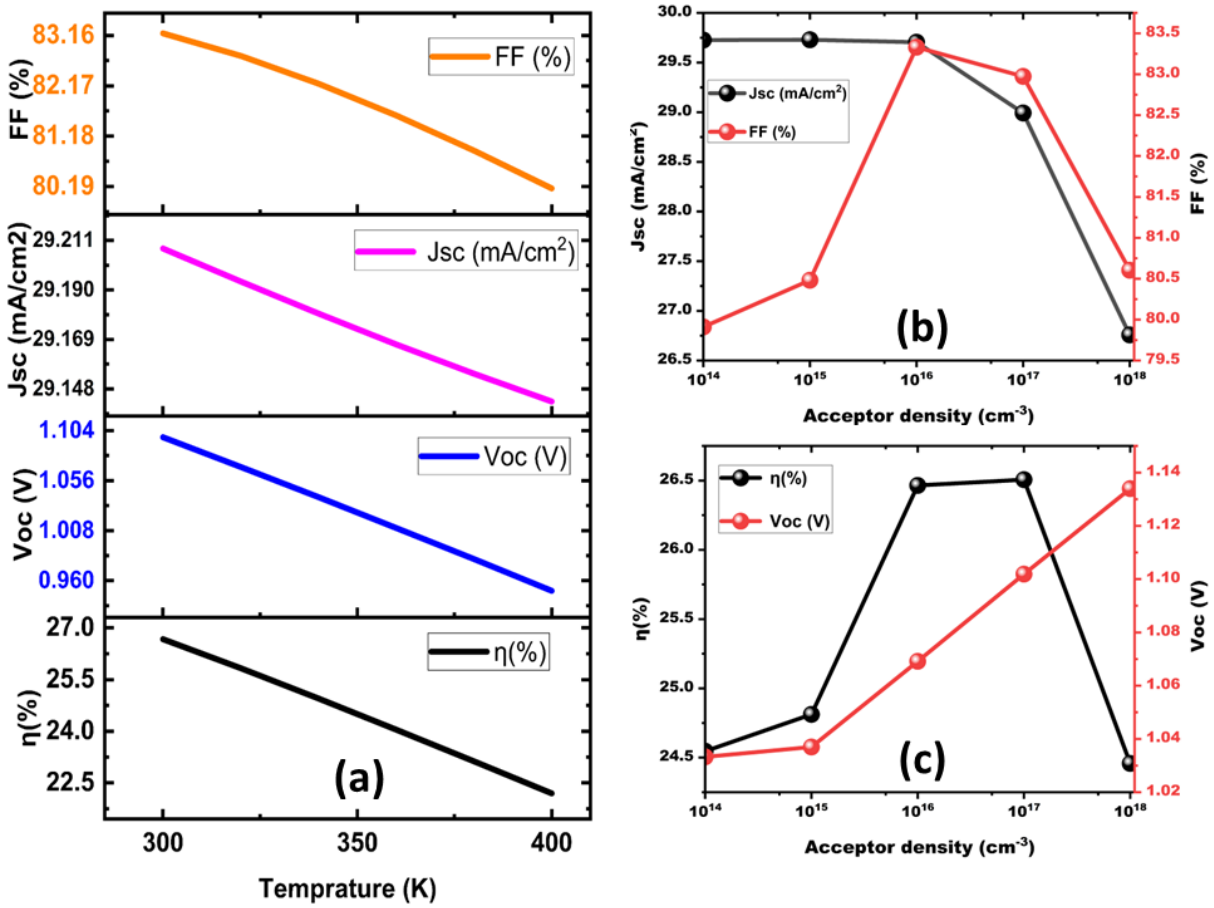

Fig 14. (a) Impact of temperature on PV parameters, **(b)** & **(c)** effect of acceptor density of absorber layer on PV parameters.

Where, $E_g\,(T)$ represents band gap energy at the temperature $T\,(K)$, and $E_g\,(0)$ represents the band gap energy at absolute zero temperature. The constants α and β are material-specific parameters, with α indicating the temperature dependence of the band gap (in eV/K) and β describing the characteristic temperature behaviours (in K) [89]. The temperature coefficient of the proposed device structure is - 0.15 % K^{-1} calculated with the help of equation (15) confirm that the device exhibits sufficient thermal stability for outdoor applications [90].

$$C_T = \left(\frac{1}{\eta_{STC}} \cdot \frac{d\eta_T}{dT} \times 100\,\%\right) \tag{15}$$

Here C_T, η_{STC}, and $d\eta_T$ are the temperature coefficient, efficiency at standard test condition (STC), and the difference in efficiency at any desired temperature T respectively. Figure 14 (b & c) depicts the effect of acceptor density of absorber layer on the PV parameters of the solar cell. As the acceptor density (N_A) increases from 10^{14}-10^{18} cm^{-3}, the short-circuit current density (J_{SC}) remains nearly constant between 10^{14} and 10^{16} cm^{-3}, then decreases from 10^{16} to 10^{18} cm^{-3}. This J_{SC} decrease with increasing N_A is attributed to factors like

increased recombination rates, reduced depletion width, and shorter minority carrier diffusion lengths [91][92]. Higher acceptor doping concentration (N_A) in the semiconductor material of a solar cell leads to an increased built-in potential and decreased saturation current density, resulting in a greater V_{OC} [93]. The efficiency (η) and fill factor (FF) of the device display a non-monotonic trend as the acceptor doping density increases. Initially, both η and FF improve with rising acceptor concentrations. This enhancement is primarily due to the increase in V_{OC}, which benefits from higher doping levels that facilitate better charge separation and enhance the built-in potential. However, as the acceptor doping density exceeds an optimal threshold, both efficiency and fill factor gradually decline. This downturn is well-documented in the literature [94] and is linked to several adverse effects associated with excessive doping. At high doping concentrations, the increased density of defect states and heightened impurity scattering significantly raise the recombination rate of charge carriers. Additionally, the carrier lifetime is notably shortened due to enhanced Auger recombination and Shockley-Read-Hall (SRH) recombination mechanisms. These factors collectively reduce charge collection efficiency, leading to a decline in overall device performance, despite the initial improvements in V_{OC}. Thus, while moderate acceptor doping enhances photovoltaic parameters, excessive doping leads to counterproductive effects such as shortened carrier life time, increased scattering, enhanced Auger and Shockley-Read-Hall (SRH) recombination mechanisms that ultimately limit the efficiency and fill factor of the device. Authors found the optimised value of the acceptor density of 7.0 x 10^{16} cm^{-3} which is possible to achieve in real life according to literatures [95][96][97].

4.5 Impact of series and shunt resistance

The performance of a PVC is strongly influenced by the parasitic resistances namely series resistance (R_s) and shunt resistance (R_{sh}). Series resistance represents the internal resistance within a solar cell, arising from the flow of current through its layers, metal contacts, and interconnections, leading to voltage drops and power losses that reduce fill factor and efficiency. Conversely, shunt resistance is associated with leakage pathways caused by defects or impurities, offering alternate routes for current that diminish voltage and overall efficiency [98]. In this study authors systematically varied the R_s from 0.5 Ω to 4.0 Ω and R_{sh} from 10^1 Ω to 10^8 Ω and find out optimised values of R_s and R_{sh} to be 0.5 Ω and 10^3 Ω respectively. Figure 15 demonstrates that these changes in resistance have a significant impact on key performance parameters of the device. Specifically, the

efficiency changes from 27.70% to 1.50%, while the FF changes from 86.20% to 25.00%. Furthermore, the Voc changes from 1.1 V to 0.29 V, and Jsc changes from 29.24 mA/cm² to 20.86 mA/cm². An increase in R_S results in greater power dissipation within the solar cell, negatively impacting its efficiency. In contrast, a higher R_{sh} is advantageous as it minimizes leakage currents and improves overall performance. The series resistance R_S is basically sum of resistance due to all components that come in the path of current including all the layers, semiconductor-metal contact resistance and resistance of metal contacts. The shunt resistance is because of the leakage of current across the P-N junction, it could be due to shunt around the periphery of the cell, due to crystal defect or precipitates of impurities in the junction region [99]. Thus, achieving low R_S and high R_{sh} is essential for optimizing efficiency. Low R_S values can be achieved by surface passivation [100], doping optimization [101] and improved contact engineering [102]. High R_{sh} values can be achieved by using high quality pin hole-free films by optimizing deposition conditions[103] and by using passivation layers to block leakage paths [104]. However, while R_{sh} may theoretically approach infinity and R_S may tend toward zero, practical limitations arise from the inherent characteristics of the solar cell's diode, which prevent these ideal conditions from being fully realized [39].

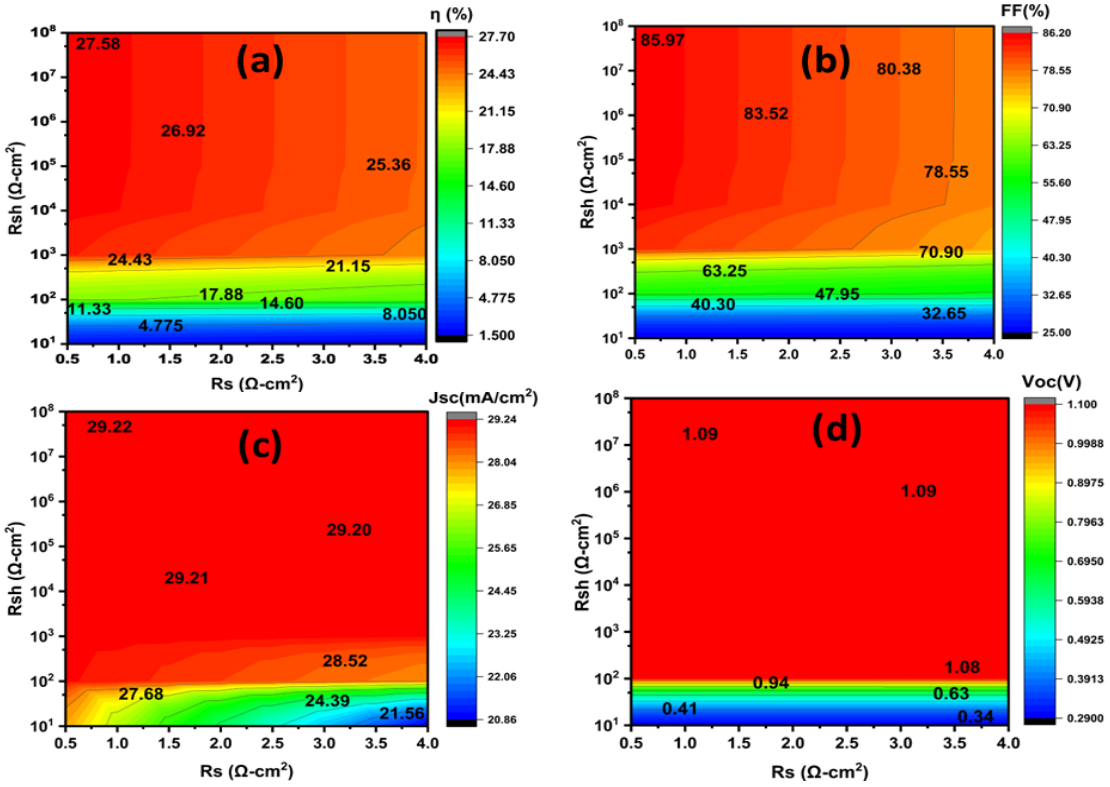

Fig 15. Effect of shunt and series resistance on **(a)** efficiency, **(b)** fill factor, **(c)** current density and **(d)** voltage

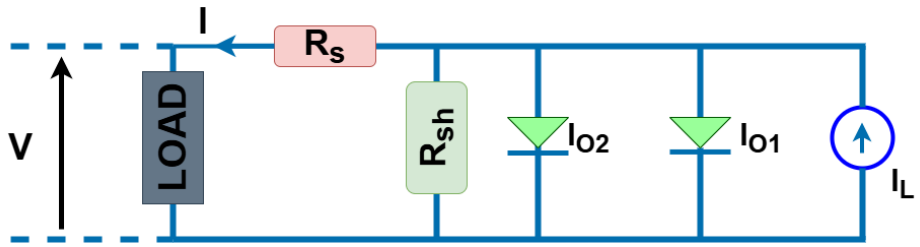

Fig 16. Equivalent diode model circuit of the solar cells.

J-V equation for an Ideal solar cell is given by:

$$J = J_L - J_O\left(exp^{\frac{qV}{kT}} - 1\right) \quad \text{eq. (16)}$$

After considering R_{SH} and R_S, the J-V equation becomes:

$$J = J_L - J_{O1}\left(exp^{\frac{q(V+IR_S)}{nkT}}\right) - \frac{V+IR_S}{R_{SH}} \quad \text{eq. (17)}$$

Where, J_{O1} is recombination in base & emitter, q is charge, V is potential, k is Boltzmann constant and R_S and R_{SH} are series and shunt resistance respectively.

The equivalent diode model circuit of the solar cells is shown in figure 6 in which solar cell is taken as current source where the current produced is directly proportional to the irradiance. One diode signifies recombination in the bulk and emitter region (including surfaces) of the cell, whilst the second diode denotes recombination in the cell's depletion region. As R_S is resistance offered by the solar cell in the path of current flow, that is why R_S is shown in the current path. The R_{SH} is referred as leakage path of the current in a solar cell, that is why it is represented in parallel with the current source [99].

4.6 Impact of interface defect density and total defect density

Figure 17. (a) shows the effect of interface defect density on the PV parameters of the simulated solar cell. In this study, authors have considered interface defect density of the HTL (CBTS)/Absorber Layer ($FASnI_3$). Interface defect density is varied from 10^{11} to 10^{17} cm^{-3} and it is clearly notice that all the PV parameters decrease with the increase in the interface defect density. An increase in interface defect density leads to enhanced charge carrier recombination and trapping (charge carriers getting captured and immobilized by localized defect states), which adversely affects photovoltaic (PV) performance. This degradation manifests as reductions in V_{OC}, J_{SC}, FF, and η.

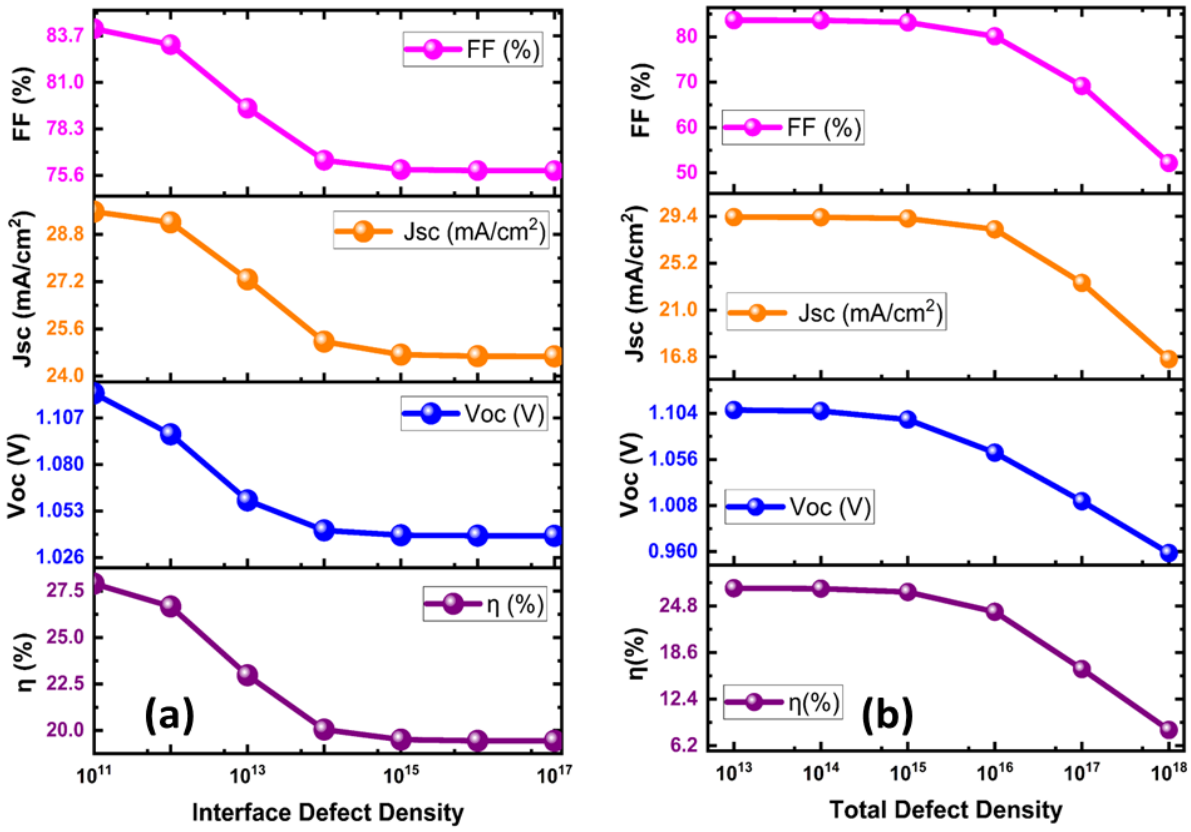

Fig 17. Effect of **(a)** interface defect density (HTL/Absorber layer) and **(b)** total defect density of absorber layer on PV parameters

The reducing of photovoltaic (PV) performance primarily arises from increased resistive losses and diminished carrier mobility. However, when defect density exceeds a critical threshold, these losses reach saturation, as the majority of charge carriers have already undergone trapping or recombination. Beyond this point, further increases in defect density contribute negligibly to the overall decline in device performance[105][106]. Figure 17. (b) shows the result of variation of total defect density of the absorber layer ($FASnI_3$). Total defect density has been varied from 10^{13} to 10^{18} cm^{-3}. Evidently, all of the PV parameters show large reduction with the increase in the total defect density. Elevated defect density in the absorber layer of a photovoltaic (PV) device enhances Shockley-Read-Hall (SRH) recombination, reducing charge carrier lifetime and collection efficiency [107]. This degradation manifests as a decline in V_{OC} due to suppressed quasi-Fermi level splitting, a reduction in J_{SC} from impaired carrier mobility and increased trapping, and a diminished FF owing to higher series resistance and inefficient charge transport. Collectively, these effects deteriorate the PCE, underscoring the necessity of defect mitigation for optimal PV performance [108].

4.7 Impact of Electron Affinity and C-V analysis

Figure 18. (a) shows the effect of electron affinity of the absorber layer on the PV parameters of the simulated solar cell. The electron affinity (χ) of the absorber layer in a photovoltaic (PV) cell is crucial for device performance due to its effects on band alignment, charge carrier transport, and recombination dynamics. An increase in χ lowers the conduction band minimum (CBM), which reduces the built-in potential (V_{bi}) and consequently affects the open-circuit voltage (V_{oc}) negatively. On the other hand, a decrease in χ creates energetic barriers at the interface with the electron transport layer (ETL), hindering electron extraction and resulting in lower J_{sc} and FF[109]. $FASnI_3$ with electron affinity of 4.0 [110] is the most used lead-free perovskite absorber layer and is preferred over $MASnI_3$ because of its better stability and electrical properties [111]. To optimize power conversion efficiency (PCE), it is essential to identify an optimal χ value that promotes effective charge collection while minimizing interfacial recombination losses. Moreover, achieving precise band alignment between the absorber layer and the ETL is critical for eliminating energy barriers, which facilitates smooth charge transport and enhances overall device performance [112]. Electron affinity has been varied from 3.60 to 4.00 and it can be clearly observed that the performance of the simulated solar cell peaked at around 3.80, making it the suitable electron affinity value for the perovskite absorber layer material. Figure 18(b)& 18(c) shows the impact of capacitance and Mott–Schottky characteristics respectively derived from C–V analysis conducted at a fixed frequency of 1 MHz. We examined the depletion and diffusion capacitances associated with p-n junctions. Under forward bias, diffusion capacitance is the dominant factor, whereas in reverse bias, depletion capacitance becomes more significant [113]. In Figure 8(b), the zero-bias capacitance of the p–n junction solar cell is measured to be approximately 40 nF/cm². At a fixed frequency (1 MHz for this simulation) and increasing polarization potential, the capacitance exhibits an exponential rise, indicating the insensitivity of absorber traps to frequency variations. Efficient charge traps exhibit minimal reduction in effective charge under reverse bias, leading to suppressed capacitance. The built-in potential (or flat-band potential, V_{bi}) of the PVC is determined by extrapolating the linear region of the $1/C^2$ vs. Voltage plot to the voltage axis (where $1/C^2 = 0$) [114]. From figure 8 (c), the built-in potential (V_{bi}) for the simulated solar cell comes out to be 0.956 V.

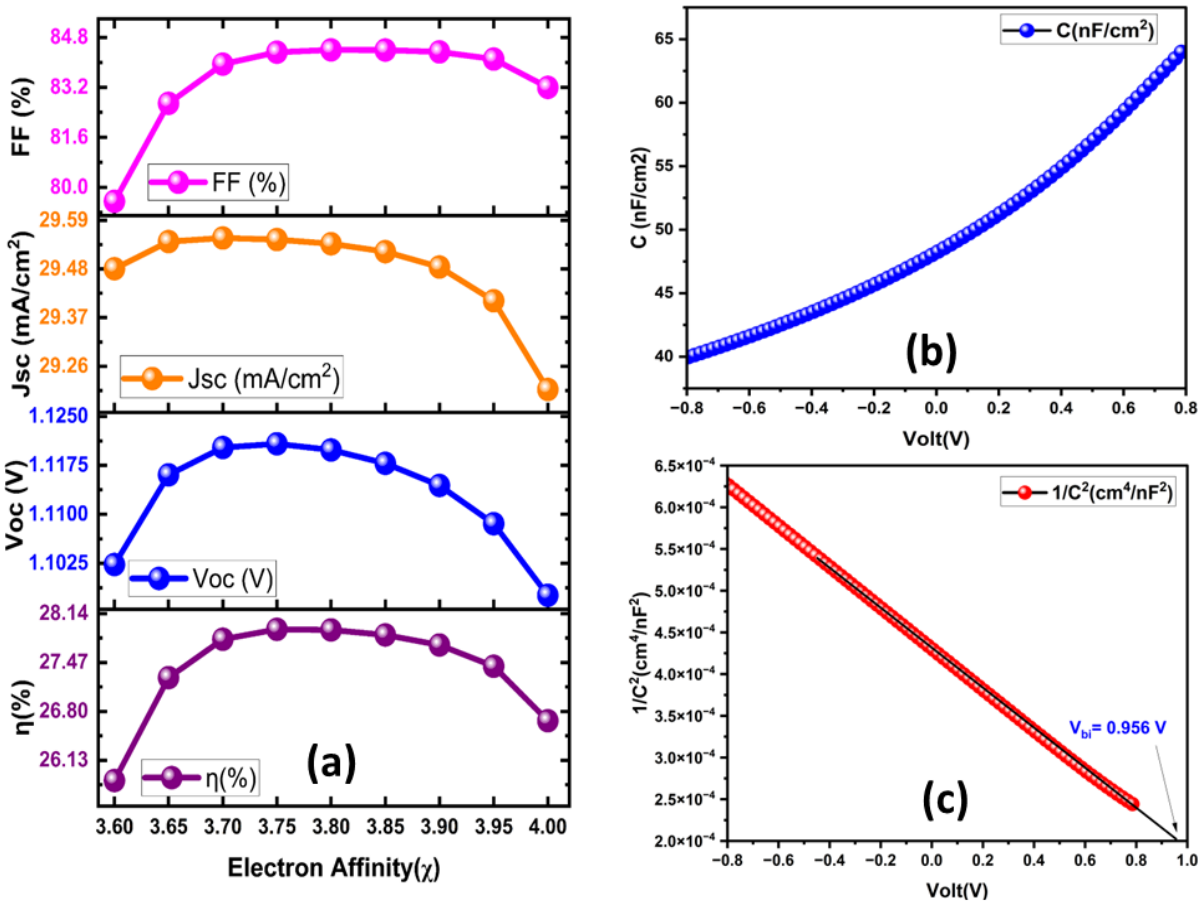

Fig 18. (a) Effect of electron affinity on PV parameters, (b) C-V characteristics (c) Mott-Schottky plot.

4.8 Effect of radiative recombination coefficient

Radiative recombination is a critical process in solar cells that significantly influences their overall performance and efficiency [115]. This phenomenon occurs when electrons and holes within the photovoltaic material recombine and release energy in the form of photons. The likelihood of this radiative recombination taking place is quantified by the radiative recombination coefficient, which serves as a key parameter in assessing the material's optoelectronic properties.

Total recombination is given by equation (18):

$$R_{\text{total}} = \frac{np - n_i^2}{\tau_n(p + h_o) + \tau_p(n + e_o)} + B(np - n_i^2) + [(np - n_i^2)(A_n n + A_p p)] \quad (18)$$

In the equation, 1st term represents SRH recombination, 2nd term represents radiative recombination and 3rd term represents Auger recombination. Here n and p are electron and hole density, e_o and h_o are electron and hole dwelling at defect level, τ_n and τ_p represent electron and hole life times, A_n and A_p are coefficient of Auger recombination and B is

radiative recombination coefficient [116]. Understanding the impact of this coefficient on PV parameters such as V_{OC}, J_{SC}, FF, and η is essential for optimizing solar cell design. By analysing its effects, the optimal radiative recombination coefficient value can be determined to maximize the device's performance. $FASnI_3$ faces challenges that exacerbate recombination losses. One major issue is the oxidation of tin from its Sn^{2+}state to Sn^{4+} state, which introduces detrimental effects on the solar cell's operation. This oxidation process increases the majority carrier concentration, accelerating the recombination of photogenerated charge carriers. Additionally, the perovskite layer can develop metallic characteristics because charge carrier concentration increases as Sn^{2+} transforms into Sn^{4+} by releasing 2 holes in valance band in this degradation, leading to a reduction in shunt resistance [117]. A lower shunt resistance facilitates leakage currents, further diminishing the solar cell's efficiency and stability. Therefore, mitigating these recombination pathways particularly by controlling the radiative recombination coefficient and minimizing non-radiative losses is crucial for advancing the development of efficient and durable Sn-based PSCs[118].

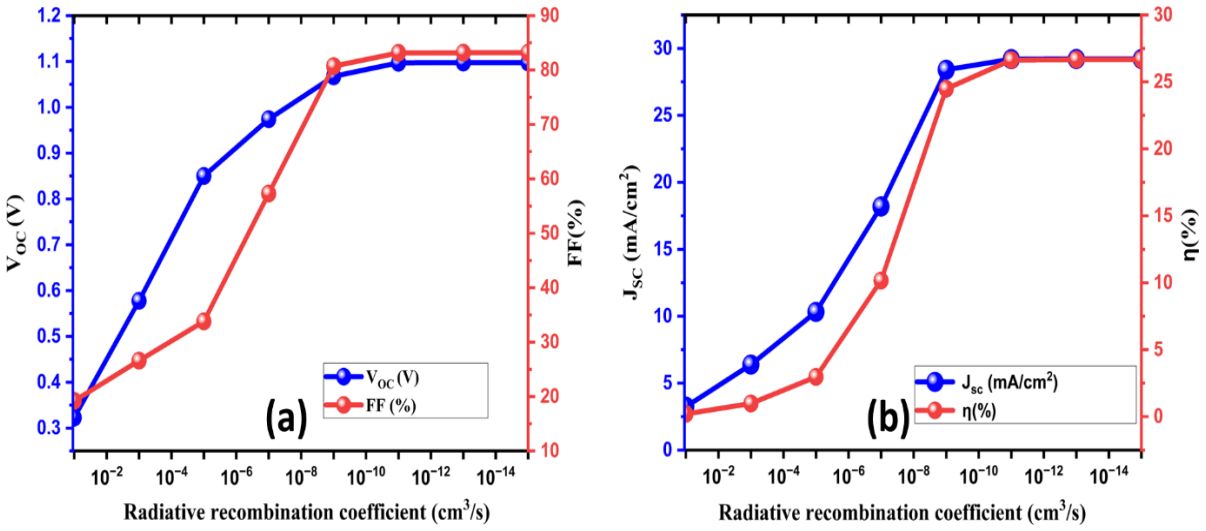

Fig 19. (a) Impact of radiative recombination coefficient on J_{SC} and η (%) and **(b)** Impact of radiative recombination coefficient on V_{OC} and FF.

In this simulation, radiative recombination coefficient has been varied from 10^{-1} cm^3/s to 10^{-15} cm^3/s. Here it is noticed that all of the PV parameters get saturated at about 10^{-12} cm^3/s shows the optimised value of radiative recombination coefficient. All of the PV parameters get saturated with increasing value of radiative recombination coefficient in accordance with the Shockley-Queisser (SQ) limit [119]. In an ideal solar cell at equilibrium, detailed balance dictates equal rates of photon absorption and emission.

Consequently, the Shockley-Queisser (SQ) limit defines the maximum theoretical η (~ 33%) of a single-junction (1N) solar cell, considering only radiative recombination. Beyond this limit, the cell re-emits photons as rapidly as it absorbs them, and further increases in the radiative recombination coefficient have no impact on efficiency and other PV parameters [120].

Table 2. Comparison between present work and work done by other researchers

Device structure	Efficiency	References
Al/FTO/WS_2 /$FASnI_3$ /Zn_3P_2 /Ni	29.81%	[121]
ITO/ZnSe/ $FASnI_3$/Cu_2O/Au	32.13 %	[122]
FTO/CeO_2/$FASnI_3$/CuI/Au	24.87%	[95]
Ag/ Spiro-OMeTAD/$FASnI_3$/TiO_2/FTO	32.47%	[123]
FTO/Zn(O0.3, S0.7)/$FASnI_3$/CuSCN/Au	14.46%	[124]
FTO/TiO_2/$FASnI_3$/ Spiro-OMeTAD /Au	15.21 %	[125]
FTO/ SnO_2/$FASnI_3$/CuI/Au	30.33 %	[126]
ITO/CeO_2/$FaSnI_3$/PTAA/Au	39.24%	[96]
FTO/TiO_2/$FASnI_3$/Spiro-OMeTAD/Au	14.03%	[127]
FTO/CeO_2/$FASnI_3$/CuI/Au	23.86 %	[128]
FTO/TiO_2/$FASnI_3$/Spiro-OMeTAD/Ag	22.49%	[129]
FTO/ TiO_2/$FASnI_3$/ Spiro-OMeTAD/Ag	18.11%	[74]
GO/$FASnI_3$/TiO_2/ZnO/ITO	20.39%	[130]
Au/CBTS/$FASnI_3$/TiO_2/FTO/Al	26.67%	This Work

CHAPTER 5: SUMMARY AND CONCLUSION

CHAPTER 5: SUMMARY AND CONCLUSION

5.1 Summary

The project's objective was to explore an inorganic HTL for $FASnI_3$ perovskite solar cells other than the usually used organic HTLs like Spiro-OMeTAD and PEDOT: PSS. In this work of scientific inquiry, systematic optimization of tin-based Pb-free perovskite solar cell with CBTS employed as HTL has been done. Aim is to numerically analyse the proposed novel solar cell structure: Au/CBTS/FASnI3/TiO2/FTO/Al and to optimize its photovoltaic performance using SCAPS-1D simulator. To achieve this goal, a comprehensive study was done, impact of several factors on the photovoltaic parameters on the proposed novel solar cell structure was examined.

First of all, J-V curve was analysed and impact of thickness of absorber layer on J-V curve and internal quantum efficiency was investigated. Then, energy band diagram of the solar cell was rigorously analysed, importance of band alignment at 3 different heterojunctions namely CBTS/$FASnI_3$, $FASnI_3$/TiO_2, and TiO_2/FTO was acknowledged. VBOs for these heterojunctions are found to be −0.9 eV, +1.9 eV, and +0.2 eV, respectively and CBOs are found to be +0.4 eV, −0.1 eV, and +0.1 eV respectively. Later, impact of work function was investigated to find out that Aluminium (Al) and gold (Au) were best suited materials for the front and back contact electrodes, respectively. Effect of temperature was studied and the thermal coefficient of -0.15% K^{-1} was calculated for the proposed solar cell which indicates strong suitability for outdoor applications. Effect of acceptor density was analysed to conclude that optimised value of the acceptor density is 7.0×10^{16} cm^{-3}, which is quite possible to achieve in real life. Effect of values of parasitic resistance (R_S and R_{SH}) on the photovoltaic parameters was studied and optimised values for R_S and R_{SH} came out to be R_{sh} to be 0.5 Ω and 10^3 Ω respectively. Equivalent diode model circuit of the solar cells was also analysed during the study. Continuous decline was observed in photovoltaic parameters while increasing both total defect density and interface defect density respectively. Later, impact of Electron affinity was examined and it was clearly seen that the all-PV parameters of the simulated solar cell peaked at around 3.80, making most used lead-free perovskite material $FASnI_3$ (with electron affinity of 4.0) to be suitable for this proposed structure. C-V analyses were also conducted for the

proposed structure by the authors and built-in potential (V_{bi}) of 0.956 V was calculated from the observed Mott-Schottky plot. Lastly, impact of radiative recombination was analysed and it was concluded that the highest performance was observed at a radiative recombination coefficient of 10^{-12} cm^3/s. Finally, the optimized structure of solar cell: Au/CBTS/FASnI3/TiO2/FTO/Al gives efficiency of 26.67% and fill factor (FF), J_{SC} and V_{OC} comes out to be 83.20%, 29.61 mA/cm^2 and 1.126 V respectively.

5.2 Conclusion and Future Scope

The importance of renewable energy sources in this world where pollution and other climate changes are increasing continuously, has been discussed. All the renewable energy sources were discussed and how solar energy holds so much potential among all the renewable energy sources has also been emphasised. The working principle of solar cells and all the four generations were concluded in the project. Further, perovskite solar cells were discussed in detail and its structure was also studied. Finally, a detailed SCAPS 1D simulation study was done for $FASnI_3$ perovskite solar cell with CBTS as HTL layer.

This comprehensive study and its results confirm that CBTS is an finely convincing HTL for FASnI3-based perovskite solar cells, while also setting the stage for exploration of more possible HTL materials and the development of high-performance, cost-effective perovskite photovoltaic devices. This study opens up future scopes for discovering and studying more stable new materials other than generally used organic materials that could be compatible as HTL with $FASnI_3$ absorber layer. This will increase the life time of the solar cell and will contribute to future of perovskite solar cells.

References

[1] "Renewable Energy - Sources, Definition, Examples, Facts." Accessed: May 14, 2025. [Online]. Available: https://www.priyamstudycentre.com/2020/11/renewable-energy.html

[2] T.-Z. Ang, M. Salem, M. Kamarol, H. S. Das, M. A. Nazari, and N. Prabaharan, "A comprehensive study of renewable energy sources: Classifications, challenges and suggestions," *Energy Strateg. Rev.*, vol. 43, p. 100939, 2022, doi: https://doi.org/10.1016/j.esr.2022.100939.

[3] R. Jones-Albertus, W. Cole, P. Denholm, D. Feldman, M. Woodhouse, and R. Margolis, "Solar on the rise: How cost declines and grid integration shape solar's growth potential in the United States," *MRS Energy Sustain.*, vol. 5, p. E4, 2018, doi: DOI: 10.1557/mre.2018.4.

[4] T. Güney, "Solar energy, governance and CO2 emissions," *Renew. Energy*, vol. 184, pp. 791–798, 2022, doi: https://doi.org/10.1016/j.renene.2021.11.124.

[5] O. Prakash *et al.*, "The compressive study of energy security prospects in India through solar power," *Int. J. Low-Carbon Technol.*, vol. 17, pp. 962–979, Feb. 2022, doi: 10.1093/ijlct/ctac075.

[6] "Solar RRL - 2023 - Jost - Integrated Micro-Scale Concentrating Photovoltaics A Scalable Path Toward High-Efficiency .pdf."

[7] C. J. Rhodes, "Solar energy: Principles and possibilities," *Sci. Prog.*, vol. 93, no. 1, pp. 37–112, 2010, doi: 10.3184/003685010X12626410325807.

[8] P. K. Nayak, S. Mahesh, H. J. Snaith, and D. Cahen, "Photovoltaic solar cell technologies: analysing the state of the art," *Nat. Rev. Mater.*, vol. 4, no. 4, pp. 269–285, 2019, doi: 10.1038/s41578-019-0097-0.

[9] N.-G. Park and K. Zhu, "Scalable fabrication and coating methods for perovskite solar cells and solar modules," *Nat. Rev. Mater.*, vol. 5, no. 5, pp. 333–350, 2020, doi: 10.1038/s41578-019-0176-2.

[10] S. Shittu, G. Li, Y. G. Akhlaghi, X. Ma, X. Zhao, and E. Ayodele, "Advancements

in thermoelectric generators for enhanced hybrid photovoltaic system performance," *Renew. Sustain. Energy Rev.*, vol. 109, pp. 24–54, 2019, doi: https://doi.org/10.1016/j.rser.2019.04.023.

[11] D. V Kumar and M. John, "A Review on Solar Tracking Methods," *IOP Conf. Ser. Mater. Sci. Eng.*, vol. 912, p. 42045, Sep. 2020, doi: 10.1088/1757-899X/912/4/042045.

[12] L. Fraas, "Chapter 1: History of Solar Cell Development," 2014. doi: 10.1007/978-3-319-07530-3_1.

[13] "The Nobel Prize in Physics 1921 - NobelPrize.org." Accessed: Apr. 19, 2025. [Online]. Available: https://www.nobelprize.org/prizes/physics/1921/summary/

[14] P. John, "The silicon solar cell turns 50," *J. Chem. Inf. Model.*, vol. 53, no. 9, pp. 1689–1699, 2013.

[15] N. Kant and P. Singh, "Review of next generation photovoltaic solar cell technology and comparative materialistic development," *Mater. Today Proc.*, vol. 56, pp. 3460–3470, 2022, doi: https://doi.org/10.1016/j.matpr.2021.11.116.

[16] J. Pastuszak and P. Węgierek, "Photovoltaic Cell Generations and Current Research Directions for Their Development," 2022. doi: 10.3390/ma15165542.

[17] L. O. A. Oyinkanola, O. A. Aremu, J. A. Fajemiroye, and S. O. Makinde, "A Review on the Third-Generation Solar Cells: Model, Materials, and Performance.," vol. VIII, no. 2454, pp. 60–66, 2023, doi: 10.51584/IJRIAS.

[18] D. C. Jordan, B. Sekulic, B. Marion, and S. R. Kurtz, "Performance and Aging of a 20-Year-Old Silicon PV System," *IEEE J. Photovoltaics*, vol. 5, no. 3, pp. 744–751, 2015, doi: 10.1109/JPHOTOV.2015.2396360.

[19] M. Di Sabatino, R. Hendawi, and A. S. Garcia, "Silicon Solar Cells: Trends, Manufacturing Challenges, and AI Perspectives," 2024. doi: 10.3390/cryst14020167.

[20] "File:Solar cell.png - Wikipedia." Accessed: May 14, 2025. [Online]. Available: https://en.wikipedia.org/wiki/File:Solar_cell.png

[21] “Solar Panel Construction — Clean Energy Reviews.” Accessed: May 14, 2025. [Online]. Available: https://www.cleanenergyreviews.info/blog/solar-panel-components-construction

[22] “Monocrystalline vs. Polycrystalline Solar Panels: What’s the Difference? - CNET.” Accessed: May 14, 2025. [Online]. Available: https://www.cnet.com/home/energy-and-utilities/monocrystalline-vs-polycrystalline-which-solar-panels-are-right-for-you/

[23] “Schematic arrangement of a thin film-based solar cell layers | Download Scientific Diagram.” Accessed: May 14, 2025. [Online]. Available: https://www.researchgate.net/figure/Schematic-arrangement-of-a-thin-film-based-solar-cell-layers_fig1_351677957

[24] “What Is the Principle of CIGS Solar Cells? - MJK Power- China PV Module Solar Panel Supplier.” Accessed: May 14, 2025. [Online]. Available: https://mjkpower.com/what-is-the-principle-of-cigs-solar-cells/

[25] “Flexible Film Triple-Junction GaAs Solar Cell 20.50mm.” Accessed: May 14, 2025. [Online]. Available: https://gaas.he-mu.com/flexible-film-triple-junction-gaas-solar-cell.html

[26] “AM-8701CAR Panasonic | Panasonic 190mW Amorphous Solar Cell solar panel | 664-6807 | RS.” Accessed: May 14, 2025. [Online]. Available: https://sa.rsdelivers.com/product/panasonic/am-8701car/panasonic-190mw-amorphous-solar-cell-solar-panel/6646807

[27] M. Aghaei, *A Review on Comparison between Traditional Silicon Solar Cells and Thin-Film CdTe Solar Cells*. 2012.

[28] I. M. Cells and P. Si, “Best Research-Cell Efficiencies,” p. 52.

[29] S. J. Heise, T. Taskesen, A. K. Ndoukoue Chintouo, and J. Ohland, “Which Parameters Determine the Low-Light Behaviour of CIGSSe-Based Thin-Film Solar Cells?,” *Front. Energy Res.*, vol. 10, no. September, pp. 1–7, 2022, doi: 10.3389/fenrg.2022.906093.

[30] J. Y. Kim, J.-W. Lee, H. S. Jung, H. Shin, and N.-G. Park, “High-Efficiency

Perovskite Solar Cells," *Chem. Rev.*, vol. 120, no. 15, pp. 7867–7918, Aug. 2020, doi: 10.1021/acs.chemrev.0c00107.

[31] M. Noman, Z. Khan, and S. T. Jan, "A comprehensive review on the advancements and challenges in perovskite solar cell technology," *RSC Adv.*, vol. 14, no. 8, pp. 5085–5131, 2024, doi: 10.1039/d3ra07518d.

[32] A. A. Ganesan, A. J. Houtepen, and R. W. Crisp, "Quantum Dot Solar Cells: Small Beginnings Have Large Impacts," 2018. doi: 10.3390/app8101867.

[33] C. E. Torrence, C. S. Libby, W. Nie, and J. S. Stein, "Environmental and health risks of perovskite solar modules: Case for better test standards and risk mitigation solutions," *iScience*, vol. 26, no. 1, p. 105807, 2023, doi: https://doi.org/10.1016/j.isci.2022.105807.

[34] "Perovskite Solar Cells | Department of Energy." Accessed: May 14, 2025. [Online]. Available: https://www.energy.gov/eere/solar/perovskite-solar-cells

[35] "Dye Sensitized Solar Cells: Structure and Working - Amrita Vishwa Vidyapeetham." Accessed: May 14, 2025. [Online]. Available: https://www.amrita.edu/news/dye-sensitized-solar-cells-structure-and-working/

[36] "Organic Solar Cells and Photovoltaics: Structure, Functions, Price & More." Accessed: May 14, 2025. [Online]. Available: https://www.solarsquare.in/blog/organic-solar-cells-benefits/

[37] "Quantum Dot Solar Cells Break Conversion Efficiency Record - IEEE Spectrum." Accessed: May 14, 2025. [Online]. Available: https://spectrum.ieee.org/quantum-dot-solar-cells-break-conversion-efficiency-record

[38] X. Li *et al.*, "Advances in mixed 2D and 3D perovskite heterostructure solar cells: A comprehensive review," *Nano Energy*, vol. 118, p. 108979, 2023, doi: https://doi.org/10.1016/j.nanoen.2023.108979.

[39] B. Ai, Z. Fan, and Z. J. Wong, "Plasmonic–perovskite solar cells, light emitters, and sensors," *Microsystems Nanoeng.*, vol. 8, no. 1, p. 5, 2022, doi: 10.1038/s41378-021-00334-2.

[40] R. Senthil and S. Yuvaraj, “A comprehensive review on bioinspired solar photovoltaic cells,” *Int. J. Energy Res.*, vol. 43, no. 3, pp. 1068–1081, 2019, doi: 10.1002/er.4255.

[41] G. Hodes and P. V Kamat, “Understanding the Implication of Carrier Diffusion Length in Photovoltaic Cells,” *J. Phys. Chem. Lett.*, vol. 6, no. 20, pp. 4090–4092, Oct. 2015, doi: 10.1021/acs.jpclett.5b02052.

[42] “Perovskite solar cell - Wikipedia.” Accessed: Apr. 25, 2025. [Online]. Available: https://en.wikipedia.org/wiki/Perovskite_solar_cell?utm_source=chatgpt.com

[43] “A History of Perovskite Solar Cells.” Accessed: Apr. 25, 2025. [Online]. Available: https://blog.bccresearch.com/a-history-of-perovskite-solar-cells?utm_source=chatgpt.com

[44] “History of Perovskites and Perovskite Solar Cells | Ossila.” Accessed: Apr. 25, 2025. [Online]. Available: https://www.ossila.com/pages/history-and-evolution-of-perovskites?utm_source=chatgpt.com

[45] “Goldschmidt tolerance factor - Wikipedia.” Accessed: Apr. 25, 2025. [Online]. Available: https://en.wikipedia.org/wiki/Goldschmidt_tolerance_factor

[46] “Cella fotovoltaica perovskitica - Wikipedia.” Accessed: Apr. 25, 2025. [Online]. Available: https://it.wikipedia.org/wiki/Cella_fotovoltaica_perovskitica?utm_source=chatgpt.com

[47] D. Liu and T. L. Kelly, “Perovskite solar cells with a planar heterojunction structure prepared using room-temperature solution processing techniques,” *Nat. Photonics*, vol. 8, no. 2, pp. 133–138, 2014, doi: 10.1038/nphoton.2013.342.

[48] “EPFL perovskite solar cells reach 21% efficiency | Laser Focus World.” Accessed: Apr. 25, 2025. [Online]. Available: https://www.laserfocusworld.com/detectors-imaging/article/16557983/epfl-perovskite-solar-cells-reach-21-efficiency?utm_source=chatgpt.com

[49] J. A. Christians *et al.*, “Tailored interfaces of unencapsulated perovskite solar cells for >1,000 hour operational stability,” *Nat. Energy*, vol. 3, no. 1, pp. 68–74, 2018,

doi: 10.1038/s41560-017-0067-y.

[50] T. Wu *et al.*, “The Main Progress of Perovskite Solar Cells in 2020–2021,” *Nano-Micro Lett.*, vol. 13, no. 1, pp. 1–18, 2021, doi: 10.1007/s40820-021-00672-w.

[51] “Perovskite - Wikipedia.” Accessed: Apr. 25, 2025. [Online]. Available: https://en.wikipedia.org/wiki/Perovskite?utm_source=chatgpt.com

[52] “Crystal structure of a typical black phase ABX3 perovskite. Reproduced... | Download Scientific Diagram.” Accessed: Apr. 25, 2025. [Online]. Available: https://www.researchgate.net/figure/Crystal-structure-of-a-typical-black-phase-ABX3-perovskite-Reproduced-from-14-with_fig1_370785603

[53] M. Mohan, N. P. Shetti, and T. M. Aminabhavi, “Perovskites: A new generation electrode materials for storage applications,” *J. Power Sources*, vol. 574, no. February, p. 233166, 2023, doi: 10.1016/j.jpowsour.2023.233166.

[54] I. H. Madshus and S. Olsnes, “Selective inhibition of sodium-linked and sodium-independent bicarbonate/chloride antiport in Vero cells.,” *J. Biol. Chem.*, vol. 262, no. 16, pp. 7486–7491, 1987, doi: 10.1016/s0021-9258(18)47592-8.

[55] “Goldschmidt tolerance factor - Wikipedia.” Accessed: Apr. 25, 2025. [Online]. Available: https://en.wikipedia.org/wiki/Goldschmidt_tolerance_factor?utm_source=chatgpt.com

[56] Deepika, A. Singh, U. K. Verma, and A. Tonk, “Device Structures of Perovskite Solar Cells: A Critical Review,” *Phys. Status Solidi Appl. Mater. Sci.*, vol. 220, no. 9, pp. 1–18, 2023, doi: 10.1002/pssa.202200736.

[57] Y. Li, “The Principle and Research Progress of Perovskite Solar Cells,” *Highlights Sci. Eng. Technol.*, vol. 106, pp. 347–352, 2024, doi: 10.54097/8r7hee26.

[58] L. C. Palilis *et al.*, “Inorganic and Hybrid Interfacial Materials for Organic and Perovskite Solar Cells,” *Adv. Energy Mater.*, vol. 10, no. 27, pp. 1–34, 2020, doi: 10.1002/aenm.202000910.

[59] M. Hatamvand *et al.*, “The role of different dopants of Spiro-OMeTAD hole

transport material on the stability of perovskite solar cells: A mini review," *Vacuum*, vol. 214, p. 112076, 2023, doi: https://doi.org/10.1016/j.vacuum.2023.112076.

[60] A. Kojima, K. Teshima, Y. Shirai, and T. Miyasaka, "Organometal halide perovskites as visible-light sensitizers for photovoltaic cells," *J. Am. Chem. Soc.*, vol. 131, no. 17, pp. 6050–6051, 2009, doi: 10.1021/ja809598r.

[61] J.-H. Im, C.-R. Lee, J.-W. Lee, S.-W. Park, and N.-G. Park, "6.5% efficient perovskite quantum-dot-sensitized solar cell," *Nanoscale*, vol. 3, no. 10, pp. 4088–4093, 2011, doi: 10.1039/C1NR10867K.

[62] M. M. Lee, J. Teuscher, T. Miyasaka, T. N. Murakami, and H. J. Snaith, "Efficient Hybrid Solar Cells Based on Meso-Superstructured Organometal Halide Perovskites," *Science (80-.).*, vol. 338, no. 6107, pp. 643–647, Nov. 2012, doi: 10.1126/science.1228604.

[63] P. Su *et al.*, "Pb-Based Perovskite Solar Cells and the Underlying Pollution behind Clean Energy: Dynamic Leaching of Toxic Substances from Discarded Perovskite Solar Cells," *J. Phys. Chem. Lett.*, vol. 11, no. 8, pp. 2812–2817, Apr. 2020, doi: 10.1021/acs.jpclett.0c00503.

[64] D. Fabini, "Quantifying the Potential for Lead Pollution from Halide Perovskite Photovoltaics," *J. Phys. Chem. Lett.*, vol. 6, no. 18, pp. 3546–3548, 2015, doi: 10.1021/acs.jpclett.5b01747.

[65] F. Hao, C. Stoumpos, D. Cao, R. Chang, and M. Kanatzidis, "Lead-Free Solid-State Organic-Inorganic Halide Perovskite Solar Cells," *Nat. Photonics*, vol. 8, pp. 489–494, May 2014, doi: 10.1038/nphoton.2014.82.

[66] L. Peng and W. Xie, "Theoretical and experimental investigations on the bulk photovoltaic effect in lead-free perovskites MASnI3 and FASnI3," *RSC Adv.*, vol. 10, no. 25, pp. 14679–14688, 2020, doi: 10.1039/D0RA02584D.

[67] M. K. Hossain, M. H. K. Rubel, G. F. I. Toki, I. Alam, M. F. Rahman, and H. Bencherif, "Effect of Various Electron and Hole Transport Layers on the Performance of CsPbI3-Based Perovskite Solar Cells: A Numerical Investigation in DFT, SCAPS-1D, and wxAMPS Frameworks," *ACS Omega*, vol. 7, no. 47, pp.

43210–43230, 2022, doi: 10.1021/acsomega.2c05912.

[68] M. K. Hossain *et al.*, "An extensive study on multiple ETL and HTL layers to design and simulation of high-performance lead-free CsSnCl3-based perovskite solar cells," *Sci. Rep.*, vol. 13, no. 1, pp. 1–24, 2023, doi: 10.1038/s41598-023-28506-2.

[69] M. Burgelman, K. Decock, A. Niemegeers, J. Verschraegen, and S. Degrave, "manual," 2025.

[70] A. Haseeb, H. Khan, H. Ullah, L. Li, A. Basit, and K. Boughanbour, "Exploring the efficiency and transparency in toxic and non-toxic perovskite solar cells by using SCAPS-1D," vol. 1, no. 1, pp. 1–20, 2024.

[71] E. C. Schueller, G. Laurita, D. H. Fabini, C. C. Stoumpos, M. G. Kanatzidis, and R. Seshadri, "Crystal Structure Evolution and Notable Thermal Expansion in Hybrid Perovskites Formamidinium Tin Iodide and Formamidinium Lead Bromide," *Inorg. Chem.*, vol. 57, no. 2, pp. 695–701, Jan. 2018, doi: 10.1021/acs.inorgchem.7b02576.

[72] A. Kumar, S. M. Giripunje, A. K. Patel, and S. Gohri, "Simulation study of cadmium-free CIGS solar cell for efficiency enhancement by minimizing recombination losses through back surface field mechanism," *Solid State Commun.*, vol. 394, p. 115694, 2024, doi: https://doi.org/10.1016/j.ssc.2024.115694.

[73] H. MallaHasan and Ö. Onay, "Investigation of the effect of different factors on the performance of several perovskite solar cells: a simulation study by SCAPS," *Eur. J. Eng. Sci. Technol.*, vol. 5, no. 1, pp. 20–38, Apr. 2022, doi: 10.33422/ejest.v5i1.927.

[74] I. Chabri, Y. Benhouria, A. Oubelkacem, A. Kaiba, I. Essaoudi, and A. Ainane, "SCAPS device simulation study of formamidinium Tin-Based perovskite solar Cells: Investigating the influence of absorber parameters and transport layers on device performance," *Sol. Energy*, vol. 262, no. July, p. 111846, 2023, doi: 10.1016/j.solener.2023.111846.

[75] J. Kong *et al.*, "Perovskite Solar Cells with Enhanced Fill Factors Using Polymer-

Capped Solvent Annealing," *ACS Appl. Energy Mater.*, vol. 3, no. 8, pp. 7231–7238, 2020, doi: 10.1021/acsaem.0c00854.

[76] A. H. Oishi, M. T. Anjum, M. M. Islam, and M. F. Nayan, "Impact of Absorber Layer Thickness on Perovskite Solar Cell Efficiency: A Performance Analysis," *Eur. J. Electr. Eng. Comput. Sci.*, vol. 7, no. 2, pp. 48–51, 2023, doi: 10.24018/ejece.2023.7.2.520.

[77] U. C. Obi, D. M. Sanni, and A. Bello, "Effect of Absorber Layer Thickness on the Performance of Bismuth-Based Perovskite Solar Cells," *Semiconductors*, vol. 55, no. 12, pp. 922–927, 2021, doi: 10.1134/S1063782621040114.

[78] M. Ismail, M. Noman, S. Tariq Jan, and M. Imran, "Boosting efficiency of eco-friendly perovskite solar cell through optimization of novel charge transport layers," *R. Soc. Open Sci.*, vol. 10, no. 6, 2023, doi: 10.1098/rsos.230331.

[79] A. Mortadi, E. El Hafidi, M. Monkade, and R. El Moznine, "Investigating the influence of absorber layer thickness on the performance of perovskite solar cells: A combined simulation and impedance spectroscopy study," *Mater. Sci. Energy Technol.*, vol. 7, pp. 158–165, 2024, doi: https://doi.org/10.1016/j.mset.2023.10.001.

[80] A. Panda, C. Sudakar, and B. R. K. Nanda, "Enhancement of Quantum Efficiency in Perovskite Solar Cells Through Whispering Gallery Modes from Titanium Oxide Micro-Resonators," *Adv. Photonics Res.*, vol. 5, no. 9, 2024, doi: 10.1002/adpr.202300339.

[81] E. Danladi, C. U. Achem, I. O. Echi, S. U. Michael, and M. E. Oni, "Thickness Variation Study of Perovskite Layer Over the Range 100-1300 nm and Its Influence on the Performance of Perovskite Solar Cells Using SCAPS Software," *J. Nano Mater. Sci. Res.*, vol. 1, pp. 22–27, 2022, [Online]. Available: https://journals.nanotechunn.com/jnmsr/article/view/5

[82] Mamta, K. K. Maurya, and V. N. Singh, "Efficient Sb2Se3 solar cell with a higher fill factor: A theoretical approach based on thickness and temperature," *Sol. Energy*, vol. 230, pp. 803–809, 2021, doi: https://doi.org/10.1016/j.solener.2021.11.002.

[83] M. K. Sobayel *et al.*, “Efficiency enhancement of CIGS solar cell by cubic silicon carbide as prospective buffer layer,” *Sol. Energy*, vol. 224, pp. 271–278, 2021, doi: https://doi.org/10.1016/j.solener.2021.05.093.

[84] P. R. Schwoebel, M. S. Salem, M. Okil, A. Shaker, A. Albaker, and M. Alturki, “Design of n-i-p and p-i-n Sb 2 Se 3 solar cells : role of band alignment Journal of Physics : Energy OPEN ACCESS Design of n-i-p and p-i-n Sb 2 Se 3 solar cells : role of band alignment,” 2023.

[85] X. Rong *et al.*, “Impact of metal electrode work function of CH3NH3PbI3/p-Si planar heterojunction perovskite solar cells,” *Sol. Energy*, vol. 158, no. May, pp. 424–431, 2017, doi: 10.1016/j.solener.2017.08.050.

[86] M. U. Salman *et al.*, “Influence of acceptor/donor densities and layer thicknesses on the efficiency of 2D ZnO/BFO/spiro-OMeTAD perovskite solar cells: a COMSOL simulation-based optimization,” *J. Mater. Chem. A*, 2025, doi: 10.1039/D4TA08899A.

[87] P. Singh and N. M. Ravindra, “Temperature dependence of solar cell performance - An analysis,” *Sol. Energy Mater. Sol. Cells*, vol. 101, pp. 36–45, 2012, doi: 10.1016/j.solmat.2012.02.019.

[88] E. T. Mohamed, A. O. M. Maka, M. Mehmood, Al. M. Direedar, and N. Amin, “Performance simulation of single and dual-junction GaInP/GaAs tandem solar cells using AMPS-1D,” *Sustain. Energy Technol. Assessments*, vol. 44, no. February, p. 101067, 2021, doi: 10.1016/j.seta.2021.101067.

[89] N. M. Ravindra and V. K. Srivastava, “Temperature dependence of the energy gap in semiconductors,” *J. Phys. Chem. Solids*, vol. 40, no. 10, pp. 791–793, 1979, doi: https://doi.org/10.1016/0022-3697(79)90162-8.

[90] O. Dupré, R. Vaillon, and M. A. Green, “Physics of the temperature coefficients of solar cells,” *Sol. Energy Mater. Sol. Cells*, vol. 140, pp. 92–100, 2015, doi: 10.1016/j.solmat.2015.03.025.

[91] J. Hüpkes, U. Rau, and T. Kirchartz, “Dielectric Junction: Electrostatic Design for Charge Carrier Collection in Solar Cells,” *Sol. RRL*, vol. 6, no. 1, p. 2100720, Jan. 2022, doi: https://doi.org/10.1002/solr.202100720.

[92] L. A. Kosyachenko, “Possibilities to decrease the absorber thickness reducing optical and recombination losses in CdS/CdTe solar cells,” *Mater. Renew. Sustain. Energy*, vol. 2, no. 3, p. 14, 2013, doi: 10.1007/s40243-013-0014-1.

[93] P. E. Pepa, D. Afungchui, O. Holtomo, and J. Ebobenow, “Parameters critically affecting the open circuit voltage of an organic solar cell,” *Heliyon*, vol. 11, no. 4, Feb. 2025, doi: 10.1016/j.heliyon.2025.e42684.

[94] A. Richter, S. Glunz, F. Werner, J. Schmidt, and A. Cuevas, “Improved quantitative description of Auger recombination in crystalline silicon,” *Phys. Rev. B*, vol. Phys. Rev., p. 165202, Oct. 2012, doi: 10.1103/PhysRevB.86.165202.

[95] S. Afzal, I. Naeem, D. Bibi, and S. Ghulam, “Performance optimization of FASnI3 based perovskite solar cell through SCAPS-1D simulation Performance optimization of FASnI 3 based perovskite solar cell through SCAPS-1D simulation,” *Hybrid Adv.*, vol. 7, no. October, p. 100301, 2024, doi: 10.1016/j.hybadv.2024.100301.

[96] L. Kanouni, L. Saidi, A. Yousfi, and O. Saidani, “PERFORMANCE ENHANCEMENT VIA NUMERICAL MODELING AND OPTIMIZATION OF FASnI3 PEROVSKITE SOLAR CELL1,” *East Eur. J. Phys.*, vol. 2024-Septe, no. 3, pp. 404–415, 2024, doi: 10.26565/2312-4334-2024-3-49.

[97] M. Asaduzzaman, M. Hasan, and A. N. Bahar, “An investigation into the effects of band gap and doping concentration on Cu(In,Ga)Se2 solar cell efficiency,” *Springerplus*, vol. 5, no. 1, p. 578, 2016, doi: 10.1186/s40064-016-2256-8.

[98] P. Singh and N. M. Ravindra, “Analysis of series and shunt resistance in silicon solar cells using single and double exponential models,” *Emerg. Mater. Res.*, vol. 1, no. 1, pp. 33–38, 2012, doi: 10.1680/emr.11.00008.

[99] Chetan Singh Solanki, “Solar Photovoltaics : Fundamentals, Technologies and Applications,” no. 2, 2011.

[100] H. Li *et al.*, “Enhancing Efficiency of Perovskite Solar Cells via Surface Passivation with Graphene Oxide Interlayer,” *ACS Appl. Mater. Interfaces*, vol. 9, no. 44, pp. 38967–38976, Nov. 2017, doi: 10.1021/acsami.7b10773.

[101] M. K. Basher *et al.*, “Effect of doping profile on sheet resistance and contact resistance of monocrystalline silicon solar cells,” *Mater. Res. Express*, vol. 6, no. 8, 2019, doi: 10.1088/2053-1591/ab1e8c.

[102] G.-S. Kim, S.-H. Kim, J. Park, K. H. Han, J. Kim, and H.-Y. Yu, “Schottky Barrier Height Engineering for Electrical Contacts of Multilayered MoS2 Transistors with Reduction of Metal-Induced Gap States,” *ACS Nano*, vol. 12, no. 6, pp. 6292–6300, Jun. 2018, doi: 10.1021/acsnano.8b03331.

[103] Z. Gao, Y. Jiang, Y. Meng, M. Du, and F. Liu, “A Review of the Fabrication of Pinhole-Free Thin Films Based on Electrodeposition Technology: Theory, Methods and Progress,” 2024. doi: 10.3390/molecules29235615.

[104] M. S. Ummah, “Defect and Contact Passivation for perovskote solar cells,” *Sustain.*, vol. 11, no. 1, pp. 1–14, 2019, [Online]. Available: http://scioteca.caf.com/bitstream/handle/123456789/1091/RED2017-Eng-8ene.pdf?sequence=12&isAllowed=y%0Ahttp://dx.doi.org/10.1016/j.regsciurbeco.2008.06.005%0Ahttps://www.researchgate.net/publication/305320484_SISTEM_PEMBETUNGAN_TERPUSAT_STRATEGI_MELESTARI

[105] A. S. Chouhan, N. P. Jasti, and S. Avasthi, “Effect of interface defect density on performance of perovskite solar cell: Correlation of simulation and experiment,” *Mater. Lett.*, vol. 221, pp. 150–153, 2018, doi: https://doi.org/10.1016/j.matlet.2018.03.095.

[106] M. Abbas, X. Xu, M. Rauf, and A. K. Kyaw, “A Comprehensive Review on Defects-Induced Voltage Losses and Strategies toward Highly Efficient and Stable Perovskite Solar Cells,” 2024. doi: 10.3390/photonics11010087.

[107] T. Al Zoubi, M. Al-Gharram, and M. Moustafa, “Insights into the impact of defect states and temperature on the performance of kesterite-based thin-film solar cells,” *Optik (Stuttg).*, vol. 264, p. 169442, 2022, doi: https://doi.org/10.1016/j.ijleo.2022.169442.

[108] X. Zheng *et al.*, “Defect passivation in hybrid perovskite solar cells using quaternary ammonium halide anions and cations,” *Nat. Energy*, vol. 2, no. 7, p. 17102, 2017, doi: 10.1038/nenergy.2017.102.

[109] N. Rahman *et al.*, “Assessing the performance of MoTe2 based solar cell with Cu2O hole transport layer through device simulation,” *Discov. Mater.*, vol. 3, no. 1, p. 25, 2023, doi: 10.1007/s43939-023-00061-7.

[110] A. ul Rehman *et al.*, “Performance optimization of FASnI3 based perovskite solar cell through SCAPS-1D simulation,” *Hybrid Adv.*, vol. 7, p. 100301, 2024, doi: https://doi.org/10.1016/j.hybadv.2024.100301.

[111] L. Liang, “Advanced Science - 2017 - Liang - Lead-Free Hybrid Perovskite Absorbers for Viable Application Can We Eat the Cake and.pdf,” 2018.

[112] Q. Chen, Y. Ni, X. Dou, and Y. Yoshinori, “The Effect of Energy Level of Transport Layer on the Performance of Ambient Air Prepared Perovskite Solar Cell: A SCAPS-1D Simulation Study,” 2022. doi: 10.3390/cryst12010068.

[113] A. Kumar, S. M. Giripunje, A. K. Patel, and S. Gohri, “A comprehensive numerical simulation analysis of back surface passivated CIGS solar cells for efficiency enhancement A comprehensive numerical simulation analysis of back surface passivated CIGS solar cells for ef fi ciency enhancement”.

[114] “p-n Junctions,” in *Physics of Semiconductor Devices*, 2006, pp. 77–133. doi: https://doi.org/10.1002/9780470068328.ch2.

[115] A. Fell, T. Niewelt, B. Steinhauser, F. D. Heinz, M. C. Schubert, and S. W. Glunz, “Radiative recombination in silicon photovoltaics: Modeling the influence of charge carrier densities and photon recycling,” *Sol. Energy Mater. Sol. Cells*, vol. 230, p. 111198, 2021, doi: https://doi.org/10.1016/j.solmat.2021.111198.

[116] A. Kumar and S. M. Giripunje, “A comparative numerical simulation study of CIGS solar cells with distinct back surface field layers for enhanced performance,” *J. Phys. Chem. Solids*, vol. 197, p. 112436, 2025, doi: https://doi.org/10.1016/j.jpcs.2024.112436.

[117] “Angew Chem Int Ed - 2023 - Zhang - Mechanistic Understanding of Oxidation of Tin-based Perovskite Solar Cells and.pdf.”

[118] J. Horn, M. Scholz, K. Oum, T. Lenzer, and D. Schlettwein, “Influence of phenylethylammonium iodide as additive in the formamidinium tin iodide

perovskite on interfacial characteristics and charge carrier dynamics," *APL Mater.*, vol. 7, Mar. 2019, doi: 10.1063/1.5083624.

[119] T. Markvart, "Shockley: Queisser detailed balance limit after 60 years," *Wiley Interdiscip. Rev. Energy Environ.*, vol. 11, no. 4, pp. 1–19, 2022, doi: 10.1002/wene.430.

[120] A. Richter, M. Hermle, and S. Glunz, "Reassessment of the Limiting Efficiency for Crystalline Silicon Solar Cells," *IEEE J. Photovoltaics*, vol. 3, pp. 1184–1191, Jul. 2013, doi: 10.1109/JPHOTOV.2013.2270351.

[121] "Advcd Theory and Sims - 2024 - Khan - Investigating the Performance of FASnI3-Based Perovskite Solar Cells with Various.pdf."

[122] K. P. Mishra, B. K. Pandey, and S. Pandey, "Unveiling the potential of FASnI3 solar cells through advanced charge transport materials: A SCAPS-1D perspective," *J. Alloys Compd.*, vol. 1006, no. September, p. 176283, 2024, doi: 10.1016/j.jallcom.2024.176283.

[123] R. S. Alqurashi, "Comprehensive investigation of material properties and operational parameters for enhancing performance and stability of FASnI3-based perovskite solar cells," *Sci. Rep.*, vol. 14, no. 1, pp. 1–12, 2024, doi: 10.1038/s41598-024-67418-7.

[124] A. Tara, V. Bharti, S. Sharma, and R. Gupta, "Device simulation of FASnI3 based perovskite solar cell with Zn(O0.3, S0.7) as electron transport layer using SCAPS-1D," *Opt. Mater. (Amst).*, vol. 119, no. June, p. 111362, 2021, doi: 10.1016/j.optmat.2021.111362.

[125] P. Fasni, S. Cell, K. Dixit, and G. Ahmad, "A Simulation Study of Various ETL Layers to Design the High Performance Pb-Free perovskite (FASnI3) Solar Cell," *Indian J. Pure Appl. Phys.*, vol. 62, no. November, pp. 971–978, 2024, doi: 10.56042/ijpap.v62i11.8697.

[126] Deepika, A. Singh, U. K. Verma, and S. Ameen, "Optimization of lead-free materials-based perovskite solar cell using SCAPS-1D simulation," *J. Phys. Chem. Solids*, vol. 186, no. November 2023, p. 111817, 2024, doi: 10.1016/j.jpcs.2023.111817.

[127] S. Abdelaziz, A. Zekry, A. Shaker, and M. Abouelatta, “Investigating the performance of formamidinium tin-based perovskite solar cell by SCAPS device simulation,” *Opt. Mater. (Amst).*, vol. 101, no. January, p. 109738, 2020, doi: 10.1016/j.optmat.2020.109738.

[128] S. Afzal, I. Naeem, D. Bibi, S. Ghulam, F. Nabeel, and R. M. Obodo, “Performance optimization of FASnI 3 based perovskite solar cell through SCAPS-1D simulation,” *Hybrid Adv.*, vol. 7, no. May, p. 100301, 2024, doi: 10.1016/j.hybadv.2024.100301.

[129] T. Sékou, A. Bouich, Y. Doumbia, and B. M. Soucase, “Comparative Analysis Using SCAPS-1D Software on the Stability and,” pp. 308–320, 2024.

[130] N. Johrin, F. P. Chee, S. Nasir, and P. Y. Moh, “Numerical study and optimization of GO/ZnO based perovskite solar cell using SCAPS,” *AIMS Energy*, vol. 11, no. 4, pp. 683–693, 2023, doi: 10.3934/ENERGY.2023034.

सर मोक्षगुंडम विश्वेश्वरय्या
("भारत रत्न" पुरस्कार से सम्मानित)